JCI The Journal of Clinical Investigation

Antigen delivery targeted to tumor-associated macrophages overcomes tumor immune resistance

Daisuke Muraoka, Naohiro Seo, Tae Hayashi, Yoshiro Tahara, Keisuke Fujii, Isao Tawara, Yoshihiro Miyahara, Kana Okamori, Hideo Yagita, Seiya Imoto, Rui Yamaguchi, Mitsuhiro Komura, Satoru Miyano, Masahiro Goto, Shin-ichi Sawada, Akira Asai, Hiroaki Ikeda, Kazunari Akiyoshi, Naozumi Harada, Hiroshi Shiku

J Clin Invest. 2019. https://doi.org/10.1172/JCI97642.

Research In-Press Preview **Immunology**

Immune checkpoint inhibitors and adoptive transfer of gene-engineered T cells have emerged as novel therapeutic modalities for hard-to-treat solid tumors; however, many patients are refractory to these immunotherapies, and the mechanisms underlying tumor immune resistance have not been fully elucidated. By comparing the tumor microenvironment of checkpoint inhibition-sensitive and -resistant murine solid tumors, we observed that the resistant tumors had low immunogenicity and lacked infiltration of $CD8^+$ T cells at the tumor site. We identified antigen presentation by $CD11b^+F4/80^+$ tumor-associated macrophages (TAMs) as a key factor correlated with immune resistance. In the resistant tumors, TAMs remained inactive and did not exert antigen-presenting activity. Targeted delivery of a long peptide antigen to TAMs by using a nano-sized hydrogel (nanogel) in the presence of a Toll-like receptor agonist activated TAMs, induced their antigen-presenting activity, and thereby transformed the resistant tumors into tumors sensitive to adaptive immune responses such as adoptive transfer of tumor-specific T cell receptor-engineered T cells. These results indicate that the status and function of TAMs have a significant impact on tumor immune sensitivity and also that manipulation of TAM functions would be an effective approach for improving the efficacy of immunotherapies.

Antigen delivery targeted to tumor-associated macrophages overcomes tumor immune resistance

Authors: Daisuke Muraoka[1,2,3], Naohiro Seo[1,4], Tae Hayashi[1], Yoshiro Tahara[4,5,6], Keisuke Fujii[1], Isao Tawara[7], Yoshihiro Miyahara[1], Kana Okamori[1], Hideo Yagita[8], Seiya Imoto[9], Rui Yamaguchi[10], Mitsuhiro Komura[9], Satoru Miyano[10], Masahiro Goto[6], Shin-ichi Sawada[4,5], Akira Asai[3], Hiroaki Ikeda[2], Kazunari Akiyoshi[4,5], Naozumi Harada[1,4,11], and Hiroshi Shiku[1,4]

Affiliations:

[1]Department of Immuno-Gene Therapy, Mie University Graduate School of Medicine, Mie 514-8507, Japan. [2]Department of Oncology, Nagasaki University Graduate School of Biomedical Sciences 852-8523, Japan. [3]Center for Drug Discovery, Graduate School of Pharmaceutical Sciences, University of Shizuoka, Shizuoka 422-8526, Japan. [4]ERATO Akiyoshi Bio-Nanotransporter Project, Japan Science and Technology Agency (JST), Tokyo 102-0076, Japan. [5]Department of Polymer Chemistry, Kyoto University Graduate School of Engineering, Kyoto 615-8510, Japan. [6]Department of Applied Chemistry, Graduate School of Engineering, Kyushu University, 744 Motooka, Nishi-ku, Fukuoka 819-0395, Japan. [7]Department of Hematology and Oncology, Mie University Graduate School of Medicine, Mie 514-8507, Japan. [8]Department of Immunology, Juntendo University School of Medicine, Tokyo 113-8421, Japan. [9]Division of Health Medical Data Science, Health Intelligence Center, Institute of Medical Science, University of Tokyo, Tokyo 108-8639, Japan. [10]Laboratory of DNA Information Analysis, Human Genome Center, Institute of Medical Science, University of Tokyo, Tokyo 108-8639, Japan. [11]United Immunity, Co., Ltd., Mie 514-8507, Japan.

Address correspondence to: Daisuke Muraoka, 1-12-4 Sakamoto, Nagasaki, Nagasaki 852-8523, Japan. Phone: 81.95.819.7081. Email: dmuraoka@nagasaki-u.ac.jp. Or to: Hiroshi Shiku, 1577 Kurimamachiya-cho, Tsu, Mie 514-8507, Japan. Phone: 81.59.231.5187. Email: shiku@clin.medic.mie-u.ac.jp.

Conflict of interest: The authors declare the following competing financial interest(s): Naozumi Harada is CEO of United Immunity, Co., Ltd. The other authors have no conflicts of interest.

Abstract

Immune checkpoint inhibitors and adoptive transfer of gene-engineered T cells have emerged as novel therapeutic modalities for hard-to-treat solid tumors; however, many patients are refractory to these immunotherapies, and the mechanisms underlying tumor immune resistance have not been fully elucidated. By comparing the tumor microenvironment of checkpoint inhibition-sensitive and -resistant murine solid tumors, we observed that the resistant tumors had low immunogenicity and lacked infiltration of $CD8^+$ T cells at the tumor site. We identified antigen presentation by $CD11b^+F4/80^+$ tumor-associated macrophages (TAMs) as a key factor correlated with immune resistance. In the resistant tumors, TAMs remained inactive and did not exert antigen-presenting activity. Targeted delivery of a long peptide antigen to TAMs by using a nano-sized hydrogel (nanogel) in the presence of a Toll-like receptor agonist activated TAMs, induced their antigen-presenting activity, and thereby transformed the resistant tumors into tumors sensitive to adaptive immune responses such as adoptive transfer of tumor-specific T cell receptor-engineered T cells. These results indicate that the status and function of TAMs have a significant impact on tumor immune sensitivity and also that manipulation of TAM functions would be an effective approach for improving the efficacy of immunotherapies.

Introduction

Accumulating preclinical and clinical evidence has shown that inhibition of immune checkpoint proteins, such as cytotoxic lymphocyte associated protein 4 (CTLA-4), programmed cell death receptor 1 (PD-1), and programmed cell death receptor ligand 1 (PD-L1), can induce durable regression of solid tumors by countering the suppression of anti-tumor T cell immunity (1-5). However, as reported in non-small cell lung cancer (NSCLC), breast cancer, pancreatic cancer, and other solid tumors, the objective response rate in this type of immunotherapy ranges from 15 to 50%, indicating that many cancer patients are still refractory to checkpoint inhibition (6, 7). In addition, certain types of tumors such as prostate tumor, sarcoma, and hepatocellular carcinoma are considered totally refractory. Many efforts to reveal the reasons for this unresponsiveness have been made in the clinical setting. For instance, in melanoma patients, associations among $CD8^+$ T cell infiltration, PD-L1 expression at the tumor site, and clinical response to treatment with anti-PD-1 antibody were previously reported (8, 9). In NSCLC patients, a correlation between the efficacy of checkpoint inhibition and the number of mutations that can lead to the generation of neoantigens has been reported (10). Thus, a series of recent findings clearly indicate that the immunological environment at the tumor site influences the sensitivity of tumors to checkpoint inhibition (4, 8-13).

The mechanisms of resistance to checkpoint inhibition also have been intensively investigated using preclinical animal models by analyzing the immunological status at the tumor site in detail. For example, loss of PTEN function in cancer cells enhances the production of immunosuppressive cytokines and decreases T cell accumulation at the tumor site (14). PTEN loss also causes autophagy inhibition and thereby makes cancer cells resistant to T cell-mediated cytotoxicity. An in vivo genetic screen recently identified PTPN2 as an additional tumor intrinsic key factor in immune resistance; deletion of the *PTPN2* gene regulating the interferon (IFN)-γ pathway sensitizes cancer cells to the treatment with anti-PD-1 antibody and GVAX vaccine by increasing the

response of cancer cells to IFN-γ signaling (15). Activation of the β-catenin pathway in cancer cells results in reduced C-C motif chemokine (CCL) 4-dependent accumulation of $CD103^+$ dendritic cells (DCs) in tumors and causes the attenuation of antigen presentation to $CD8^+$ T cells by these DCs in the tumor-draining lymph node (16). Consequently, checkpoint inhibition is ineffective in this type of tumor due to the absence of tumor-specific $CD8^+$ T cells. Another study in mice treated with checkpoint inhibitors revealed a different mechanism involving DCs that may greatly affect resistance: the gut microbiome. Certain bacteria, particularly Bifidobacterium or Bacteroidales, alter DC activity in the lymph nodes, thereby contributing to the improvement of tumor-specific T cell function and influencing sensitivity to checkpoint inhibition (17, 18).

Tumor-associated macrophages (TAMs) have recently attracted attention as an important mechanism for inducing immune suppression at the tumor site. Monocytes accumulating at the tumor site in a CCL2-dependent manner differentiate to TAMs (19-21). Terminal TAM differentiation is regulated by futalic acid and intracellular Notch signaling and is characterized by the loss of Ly6c expression and gain of major histocompatibility complex (MHC) class II expression (19, 21). Differentiation to immunosuppressive M2-like MHC^{low} TAMs was shown to be associated with hypoxia (22). Interleukin (IL)-10 produced by TAMs negatively regulates the secretion of inflammatory cytokines (e.g., IL-12) from myeloid cells and promotes a Th2-type immune response (23). Arginase-1 is induced in immunosuppressive TAMs by IL-4, IL-10, and hypoxia and impairs T cell function by depleting arginine in the tumor microenvironment (24, 25). Nitric oxide production and PD-L1 expression by TAMs also suppress the T cell response. A series of recent studies reported more direct involvement of TAMs in tumor resistance to checkpoint inhibition. VISTA expressed on TAMs serves as an additional checkpoint pathway and helps tumor cells to escape from the effect of anti-PD-1 antibody (26). Thus, important roles of TAMs in the regulation of tumor immunity have been established, making TAMs a potential therapeutic target to overcome tumor immune resistance.

Some attempts to develop TAM-targeted anti-tumor drugs have focused on the depletion of TAMs using agents such as anti-CSF1R antibody (27), trabectedin (28), docetaxel (24−26), or clodronate liposome (29). Novel approaches to transform TAMs from immunosuppressive M2 phenotype to immunostimulatory M1 have also been investigated. For instance, treatment of the tumor with a PI3Kγ inhibitor was shown to switch TAMs from a M2-like phenotype to a M1-like state, leading to growth suppression of checkpoint inhibition-resistant tumors (30).

We have developed a series of nano-sized hydrogels (nanogels) to create novel nanomaterials for biomedical applications. In particular, cholesteryl pullulan (CHP), a pullulan polysaccharide partially hydrophobized by the modification with cholesteryl groups, is well established as a highly biocompatible, efficient vaccine delivery system targeting lymph node macrophages. CHP forms nanogel particles with a diameter of less than 100 nm by self-assembly (31-33). The CHP nanogel particle can efficiently entrap peptide antigens or protein antigens (34, 35). Although the CHP nanogel lacks known ligands for immune cells, surface charge, and immune stimulating activity (unpublished data), a subcutaneously injected CHP nanogel efficiently and promptly delivered antigen to lymph node macrophages with high cross-presenting activity, thereby inducing prominent antigen-specific T cell response (36).

In this study, we characterized the mechanism underlying tumor resistance to T cell immunity-dependent immunotherapies. By comparing in detail the immunological status at the tumor local site among checkpoint inhibition-resistant and -sensitive murine tumors, $CD11b^{+}F4/80^{+}$ TAMs were identified as a key factor closely correlated with such resistance. In the resistant tumors, TAMs were inactive and did not exert antigen-presenting activity. We then found that intravenously injected CHP nanogel can efficiently deliver a long peptide antigen to TAMs, and also that when accompanied by a TLR agonist such as CpG oligoDNA, TAM-targeted antigen delivery can efficiently elicit antigen presentation by TAMs. This manipulation of TAM function sensitized the resistant tumors to

T cell immunity-dependent immunotherapies, in particular, adoptive transfer of tumor-specific T cell receptor (TCR)-engineered T cells. These results indicate that TAMs play a significant role in tumor immune resistance and that manipulation of TAM function would be a promising approach for enhancing the efficacy of cancer immunotherapies.

Results

Murine CMS5a fibrosarcoma serves as a preclinical model of checkpoint inhibition-resistant tumors. To identify preclinical murine tumor models refractory to immune checkpoint inhibition, we treated several syngeneic murine tumors subcutaneously implanted into BALB/c mice with checkpoint inhibitors, including anti-PD-1 (37, 38), anti-CTLA-4 (38-40), and anti-GITR antibodies (41, 42) on days 7, 9, and 11 after tumor inoculation. The tested tumors included colon tumor CT26, fibrosarcoma CMS7, fibrosarcoma CMS5a, and CMS5a engineered to express exogenous human NY-ESO-1 protein (CMS5a/NY) (43-46). NY-ESO-1 antigen is known to be highly immunogenic (47, 48), and its forced expression was expected to make CMS5a more immunogenic. First, we examined the effect of treating these tumors with either an anti-PD-1, anti-CTLA-4, or anti-GITR antibody. Although treating with anti-CTLA-4 or anti-GITR antibodies partially inhibited growth in CT26 and CMS5a/NY tumors, the anti-PD-1 antibody was not effective (Supplemental Figure 1). Therefore, we decided to use a cocktail of these three antibodies to obtain more potent anti-tumor activity. As a result, the growth of CT26, CMS7, and CMS5a/NY tumors was strongly retarded by this treatment, indicating that these tumors are sensitive to checkpoint inhibition (Figure 1A). In contrast, the growth of CMS5a tumors was totally unaffected, indicating that CMS5a tumors are highly refractory to checkpoint inhibition (Figure 1A). A previous report showed that the efficacy of checkpoint inhibition depends, at least in part, on tumor-specific cellular responses (5). Consistent with this finding, the anti-tumor effects of checkpoint inhibitors on the CT26, CMS7, and CMS5a/NY tumors were abolished in nude mice (Figure 1B). To further examine the contribution of T cell immunity to the effect of checkpoint inhibition, we evaluated specific T cell responses towards potential neoantigens in checkpoint inhibitors-treated tumors using a combination of exome and RNA sequencing, in silico prediction of T cell epitopes, and in vitro stimulation of spleen-derived T cells with predicted, neoantigen-derived $CD8^+$ T cell epitope (neoepitope) peptides (Supplemental Tables 1–3) followed

by measuring IFN-γ or CXCL9 production (49). The mutation burden in the tested tumors was generally comparable (Supplemental Table 4). In treated CT26 tumors, specific $CD8^+$ T cell responses towards some neoepitopes and an epitope derived from endogenous murine leukemia provirus antigen (50) were detected (Figure 1C, D). Similarly, a $CD8^+$ T cell response towards a neoepitope was detected in treated CMS7 tumors (Figure 1C). In contrast, in the CMS5a and CMS5a/NY tumors, no $CD8^+$ T cell responses to the tested neoepitopes were observed, including the previously reported mutated ERK2 kinase-derived 9m epitope (51) (Figure 1C, D). However, in the CMS5a/NY tumors, a specific $CD8^+$ T cell response to the exogenous NY-ESO-1 antigen was clearly detected (Figure 1C, D). Duan et al. previously discovered that several neoantigens can act as tumor rejection antigens in the CMS5a tumors (52). Nevertheless, these neoantigen-specific $CD8^+$ T cell responses were not detected in the CMS5a tumors treated with checkpoint inhibitors (Supplemental Figure 2). Thus, no specific $CD8^+$ T cell response was detected in the CMS5a tumor model. These results indicate that highly immunoresistant CMS5a fibrosarcomas with very low immunogenicity resemble checkpoint inhibition-resistant human tumors and may be useful as a preclinical model for studying the mechanisms of immune resistance.

Tumor-associated macrophages (TAMs) are a key factor in tumor immune resistance. Previous studies demonstrated that the efficacy of checkpoint inhibitors correlates with the expression of PD-1 and T-cell immunoglobulin and mucin domain 3 (Tim3) on tumor-infiltrating lymphocytes (TILs) prior to treatment (53). The expression of killer cell lectin-like receptor G1 (KLRG1), CTLA-4, and GITR is a useful marker of $CD8^+$ T cell differentiation or activation (54-57). We therefore compared the expression of PD-1, Tim3, KLRG1, CTLA-4, and GITR on $CD8^+$ TILs and $CD4^+$ TILs from immune-sensitive and -resistant tumors. Whereas TILs frequently expressed these five markers at the significant level in two of the sensitive tumors (CT26 and CMS7), TILs in another sensitive tumor (CMS5a/NY) as well as the resistant tumor (CMS5a) expressed only CTLA-4 and GITR

(Figure 2A to D). In addition, these markers were expressed at similar levels on TILs among all four tumor models after treatment with checkpoint inhibitors (Supplementary Figure 3). In an immunohistochemical analysis, PD-1 expression at the tumor site was detected only in the CT26 tumors (Figure 2E). No clear trends were also observed in the number of $CD8^+$ TILs among sensitive and resistant tumors (Figure 2F). Thus, in our system, there was no clear relationship between the efficacy of checkpoint inhibition and the activation of TILs, suggesting the presence of other mechanisms of immune resistance.

Treated (Figure 1C, D) and untreated (Supplemental Figure 4) CMS5a tumors lacked a spontaneous T cell response specific to neoepitopes, including the mutated ERK2-derived 9m epitope. If this is a main cause of immune resistance, adoptive cell transfer (ACT) of 9m-specific T cells might suppress the growth of CMS5a tumors. To test this possibility, T cells from DUC18 mice that were genetically engineered to express a 9m-specific TCR were infused into the CMS5a tumor-bearing mice; however, the growth of CMS5a tumors was not affected (Figure 2G). In contrast, similar treatment of the CMS5a/NY tumor-bearing mice resulted in significant inhibition of tumor growth. These results indicate that the CMS5a tumors must possess other mechanism(s) of resistance.

To obtain more clues on the mechanism(s) of resistance, whole gene expression at the tumor site was investigated. mRNAs isolated from in vivo CMS5a, CMS5a/NY, CMS7, and CT26 tumors were subjected to microarray analysis. Gene set enrichment analysis (GSEA) using database-curated gene sets revealed that in the CMS5a tumors, the expression of genes induced in lipopolysaccharide (LPS)-treated bone marrow-derived macrophages (GSE-14769) (58) or in oncolytic virus-treated tumors (59) was different from that in the sensitive tumors (CT26, CMS7, and CMS5a/NY) (Figure 3A and B). Intratumoral injection of oncolytic virus is known to induce inflammatory responses, including macrophage activation. We therefore subjected mRNA of TAMs isolated from in vivo resistant and sensitive tumors to microarray analysis. GSEA identified significant differences in the

expression of genes related to inflammatory responses (60) and interferon gamma responses (60) between the sensitive tumors and the resistant tumors, indicating that TAMs in the sensitive tumors have a highly inflammatory phenotype (Figure 3C). Based on these results, we hypothesized that there may be a difference in TAM status and/or function between resistant and sensitive tumors. Indeed, TAMs in the resistant CMS5a tumors expressed PD-L1, CD40, and MHC class II at considerably lower levels compared to the sensitive tumors (CT26, CMS7, and CMS5a/NY) (Figure 3D, E), indicating that TAMs in the resistant tumors remain inactive. Antigen-presenting activity of TAMs was also compared between the immune-resistant CMS5a and the sensitive CMS5a/NY tumors. TAMs were isolated from in vivo tumors and co-cultured with $CD8^+$ T cells from 9m TCR transgenic DUC18 mice as responder cells (61). TAMs from the resistant CMS5a tumors did not stimulate DUC18 $CD8^+$ T cells, whereas those from the sensitive CMS5a/NY tumors clearly induced proliferation and IFN-γ production in antigen-specific $CD8^+$ T cells (Figure 3F). Consistent with this, TAMs from the sensitive CT26 tumor also stimulated antigen-specific T cells (Supplemental Figure 5). These data indicate that activation of and antigen presentation by TAMs are closely correlated with tumor sensitivity to checkpoint inhibition.

Inflammation at the tumor site has been reported to affect the activation of TAMs and antigen presentation by these cells (62). To understand the mechanisms contributing to TAM activation in sensitive tumors, we examined TAM activation in the sensitive CMS5a/NY tumors implanted into IFN-γ knockout mice or nude mice. As a result, upregulation of PD-L1 and MHC class II on TAMs from these mice was abrogated (Figure 4A). Again, activation of TAMs in the sensitive CMS5a/NY tumor was observed in terms of MHC class II and PD-L1 upregulation as compared to that in the resistant CMS5a tumors (Figure 4A). Depleting $CD8^+$ T cells or $CD4^+$ T cells in the CMS5a/NY tumor-bearing mice also hampered TAM activation (Figure 4B). Furthermore, antigen-presenting ability of TAMs was abrogated in the CMS5a/NY tumors implanted into IFN-γ knockout mice or

nude mice (Figure 4C). Finally, given that resistant tumors lack specific $CD8^+$ T cell responses, the presence of highly immunogenic tumor antigens in sensitive tumors stimulates $CD8^+$ TILs (and $CD4^+$ TILs), leading to TAM activation by T cell-produced inflammatory molecules such as IFN-γ and substantially affecting the sensitivity of tumors to immune attack.

Nanogel-based antigen delivery with TLR agonist induces antigen presentation by TAMs. Given that the lack of antigen presentation by inactive TAMs is closely associated with immune resistance, we speculated that manipulation of TAMs to activate antigen presentation might improve tumor sensitivity. Inactive TAMs in resistant tumors may still have the potential to present antigens (Supplemental Figure 6). To deliver tumor antigens to TAMs in vivo, we utilized a novel antigen delivery system, cholesteryl pullulan (CHP) nanogel. CHP is a pullulan polysaccharide chemically modified with cholesteryl groups and spontaneously forms a nanogel with a diameter of 20 to 50 nm via hydrophobic interactions among the cholesteryl groups in an aqueous solution (Supplemental Figure 7). CHP nanogel is an inert monodisperse nanoparticle with no electric charge (Supplemental Figure 7) and no ligands for phagocytic receptors on its surface. When subcutaneously injected, the CHP nanogel promptly accumulates in the draining lymph node and is efficiently incorporated into lymph node medullary macrophages in a highly selective manner (36). It is also known that intravenously injected nanoparticles can penetrate into tumor tissue by an enhanced permeability and retention (EPR) effect and/or stochastic eruptions (63-65). Considering this information, we speculated that after intravenous injection, a complex of CHP and tumor antigen might migrate into the tumor and might be efficiently engulfed by TAMs. We therefore prepared a complex (CHP:LPA) of a fluorescently labeled CHP nanogel and a synthetic long peptide antigen (LPA) containing the 9m epitope and tested the effects of its intravenous injection into CMS5a tumor-bearing mice. As early as 1 h after injection, accumulation of CHP:LPA in the whole tumor was observed, however CHP:LPA was not yet incorporated to TAMs or any other immune cells at this time (Figure 5A, B,

and C). At 6 and 18 h after injection, cellular uptake of CHP:LPA was obviously found in TAMs but not in T cells or B cells at the tumor site (Figure 5B and C). Incorporation of the CHP nanogel into $CD11b^{+}F4/80^{+}$ TAMs was also confirmed by immunohistochemistry (Figure 5D). Next, we investigated whether targeted antigen delivery conferred TAM antigen-presenting activity. The CMS5a tumor-bearing mice were intravenously injected with the CHP:LPA complex and a TLR9 agonist, CpG oligoDNA (ODN). TAMs were then isolated from the tumors. Antigen-presenting activity of these cells was evaluated by co-culturing with DUC18 $CD8^{+}$ T cells. TAMs from the treated mice showed potent antigen-presenting activity, whereas those from the untreated or CHP (without LPA) plus CpG ODN-treated mice did not (Figure 5E). It was not until 18 h after the injection of CHP:LPA plus CpG ODN when antigen-presenting activity of TAMs from the treated mice was detected. Interestingly, although the CHP:LPA complex was also incorporated into macrophages in other tissues (e.g., liver, lung, and spleen), macrophages in these normal tissues did not stimulate specific $CD8^{+}$ T cells (Supplemental Figure 8A, B). In DCs in the tumor-draining lymph node of treated mice, CHP:LPA incorporation and subsequent antigen presentation were not detected (Supplemental Figure 8C). Histopathological analysis showed no toxicological changes caused by the CHP:LPA complex itself in the tissues where CHP:LPA incorporation was detected, although some changes derived from CpG ODN were found in the liver and spleen of mice treated with either CpG ODN or CHP:LPA plus CpG ODN (Supplemental Figure 9). Thus, the CHP nanogel delivery system enabled the efficient and safe delivery of antigens to TAMs, thereby eliciting antigen presentation in these cells.

Induction of antigen presentation by TAMs overcomes tumor immune resistance. We next investigated whether the CHP:LPA-induced antigen presentation in TAMs would transform tumors from immune-resistant to -sensitive. Intravenous administration of the CHP:LPA and CpG ODN was nearly ineffective in the CMS5a tumors even when combined with immune checkpoint inhibitors

(Figure 6A). This result was likely due to a lack of tumor-specific $CD8^+$ T cell response induction during treatment in the non-immunogenic CMS5a tumor model: intravenous administration of the CHP:LPA and CpG ODN alone is not accompanied by de novo induction of specific T cells (Supplemental Figure 10). To establish a tumor-specific $CD8^+$ T cell response in the CMS5a tumor-bearing mice, we next infused 9m epitope-specific DUC18 $CD8^+$ T cells into the mice after intravenous injection of the CHP:LPA plus CpG ODN. As a result, injecting CHP:LPA with CpG ODN on days 7 and 11 followed by ACT of DUC18 $CD8^+$ T cells on days 8 and 12 prominently slowed the growth of CMS5a tumors, leading to rejection of these hard-to-treat, highly immune-resistant tumors (Figure 6B and C). The therapeutic effect was decreased or abolished when one of the three components was omitted (Figure 6A−C). CpG ODN was found to support TAM activation (Supplemental Figure 11). A similar synergistic effect of CHP:LPA and engineered T cell transfer was also observed in the presence of poly-IC RNA instead of CpG ODN (Supplemental Figure 12). These results suggest that intravenous administration of CHP:LPA and TLR agonist transforms solid immune-resistant tumor to immune-sensitive tumor; furthermore, when combined with engineered T cell transfer, it can eradicate immune checkpoint inhibition-resistant tumors.

To investigate the significance of TAMs in the efficacy of this novel combination immunotherapy, macrophages in the CMS5a tumor and spleen but not in the lymph node were depleted by intravenous injection of clodronate liposome (36, 66, 67) (Supplemental Figure 13). Clodronate liposome-mediated TAM depletion prior to combination immunotherapy treatment severely limited tumor growth inhibition (Figure 6D). Tumor growth was comparable between the mice treated with clodronate liposome alone and those treated with clodronate liposome and CHP:LPA plus CpG ODN. In contrast, intratumoral injection of bone marrow-derived macrophages treated in vitro with 9m epitope peptide and CpG ODN into CMS5a tumor-bearing mice resulted in improved efficacy of ACT (Figure 6E). Immunohistochemical analysis indicated the co-localization

of CHP:LPA-ingested TAMs and specific $CD8^+$ T cells at the tumor site (Figure 6F). Thus, TAMs were essential for CHP:LPA-enhanced efficacy of ACT.

The changes in the tumor local site caused by TAM-targeted antigen delivery followed by ACT was investigated 3 days after ACT. Intravenous injection of CHP:LPA clearly enhanced accumulation of infused 9m-specific $CD8^+$ T cells at the tumor site (Figure 7A). Consistent with this finding, the level of chemokines known to recruit T cells such as MIG (CXCL9), MIP-1a (CCL3), and RANTES (CCL5) at the tumor site was increased by treatment (Figure 7B). The amount of Th1-type cytokines such as IFN-γ and IL-12 was also increased (Figure 7C). These results indicate that antigen presentation by TAMs leads to the establishment of Th1 status in the tumor microenvironment and thereby efficiently enhances specific $CD8^+$ T cell infiltration. Interestingly, expression of PD-1 in tumor-infiltrating 9m-specific $CD8^+$ T cells in the combination therapy group was markedly lower than that in the ACT group or CpG ODN + ACT group (Figure 7D). A similar result was also obtained in endogenous tumor-infiltrating specific $CD8^+$ T cells in a B16 tumor-bearing mice model (38) after treatment with CHP:LPA plus CpG ODN (Supplementary Figure 14). An increased amount of the transcription factor T-bet, a repressor of PD-1 expression (68), was observed in 9m-specific $CD8^+$ T cells infiltrating in the CMS5a tumor after the intravenous injection of CHP:LPA (Supplementary Figure 15), indicating that appropriate antigen presentation at the tumor site prevents PD-1 induction on $CD8^+$ T cells via upregulation of T-bet (68).

Taken together, our data indicate that manipulation of TAMs to activate antigen presentation at the tumor site transforms resistant tumors into those sensitive towards T cell immunity. In addition, in combination with adoptive T cell transfer, TAM-targeted antigen delivery can lead to the cure of highly immune-resistant tumors.

Discussion

The present work demonstrates that TAMs are one of the key factors determining tumor immune sensitivity. In immune-resistant tumors, TAMs remained inactive and did not serve as antigen-presenting cells. However, in the presence of TLR stimulation, nanogel-mediated selective antigen delivery elicits antigen-presenting activity in TAMs. Consequently, resistant tumors become sensitive to T cell-mediated immune attack. Because TAM activation was not observed in the absence of IFN-γ or T cells, the interaction between TAMs and T cells is critical for this phenomenon. Analysis of the tumor local site after treatment confirmed the increase in tumor-infiltrating specific $CD8^+$ T cells, inflammatory cytokines, and T cell-recruiting chemokines, also indicating that the interplay between activated, antigen-presenting TAMs and specific T cells is vital for enhancement of the therapeutic activity of treatment. Consistent with our results, a previous study reported that infusion of IL-12-producing $CD8^+$ T cells induced inflammation at the tumor site and therefore the acquisition of antigen-presenting ability in myeloid cells, resulting in enhanced IFN-γ cellular responses (62).

The molecular mechanism(s) underlying the treatment-induced functional activation of TAMs is of great interest. We sought to identify transcription factor(s) responsible for the treatment-induced antigen presentation activity of TAMs. We focused on some transcription factors related to M1/M2 polarization of macrophages and compared their mRNA expression using microarray analysis between the treated and nontreated CMS5a tumors or between the sensitive CMS5a/NY tumor and resistant CMS5a tumor (Supplemental Table 5). No significant differences were detected in the levels of the tested transcription factors, implying that other molecular mechanisms such as post-translational modification of these transcription factors and/or epigenetic regulation of other macrophage-associated genes are involved in the phenomenon. To understand the mechanisms and

to obtain more clues for TAM-targeted cancer immunotherapy, we are investigating cellular and molecular events that occur in TAMs after treatment with CHP:LPA plus CpG ODN in detail.

All three components of our combination immunotherapy, i.e., CHP:LPA complex, TLR agonist, and tumor-specific receptor-engineered T cells, played indispensable roles in the efficacy of treatment. Intravenously injected CHP:LPA successfully induced antigen presentation by TAMs. To our knowledge, this is the first report of selective antigen delivery to antigen presenting cells localizing at tumor tissues. Interestingly, this modification improved tumor sensitivity towards T cell-mediated immunity, thereby rendering this approach different from conventional lymph node-targeted delivery of antigens and TLR ligands to reinforce anti-tumor T cell-mediated immunity (36, 69). A TLR agonist was also essential in the present combination immunotherapy, as macrophages that engulf antigens but are inactive cannot efficiently present antigens to T cells. Infused tumor-specific $CD8^+$ T cells were necessary for tumor regression.

TAMs, as well as myeloid-derived suppressor cells (MDSCs), have been generally recognized as suppressor cells that work locally at the tumor site, and inhibition or depletion of TAMs is therefore expected to enhance anti-tumor immune responses. However, several studies have recently proposed the modulation of the function of tumor-associated myeloid cells as a novel, effective therapeutic strategy (23, 30, 70, 71). Because macrophage-produced IL-10 inhibits the tumor-inhibitory functions of tumor-associated DCs (TADCs), treatment with anti-IL-10R antibody enhances IL-12 production from TADCs and induces potent $CD8^+$ T cell-dependent anti-tumor responses (23). By affecting TAMs, IL-12 also augments cellular immune responses, inducing tumor regression accompanied by activation of TADCs. Vaccination with LPA activates TAMs and promotes their secretion of inflammatory cytokines, thereby suppressing tumor growth (70). The treatment of tumors with PI3Kγ inhibitor was shown to switch TAMs from a M2-like phenotype to a M1-like state, leading to growth suppression of checkpoint inhibition-resistant tumor (30). Our study

revealed for the first time the importance of antigen presentation by TAMs. Recent findings along with those presented here clearly suggest that the manipulation of TAM function could provide a promising strategy to potentiate the efficacy of immunotherapy.

CHP nanogel particles have a diameter of around 40 nm (36) that is small enough to pass through the walls of lymph capillary and tumor vessels. In addition, CHP is an immunologically stealthy biomaterial, having neither immune stimulating activity, surface charge, nor known ligands. Our previous study demonstrated that when subcutaneously injected, the CHP nanogel efficiently and selectively delivers LPA to medullary macrophages in the draining lymph node; in the presence of TLR stimulation, these cells acquire the ability to present antigens to specific $CD8^+$ T cells (36). In the current study, we found that intravenously injected CHP:LPA complex preferentially accumulated in tumors rather than lymph nodes, possibly through an EPR effect and/or stochastic eruptions (63-65). It is also likely that the inertness of nanogel helps it to avoid the capture by the reticuloendothelial system and/or the extracellular matrix. This indicates that the injection route greatly affects the in vivo distribution and action of nanogel-complexed antigen. Our early cancer vaccine products containing a protein antigen and CHP nanogel have been evaluated clinically and their safety has been confirmed, indicating that the CHP nanogel is highly biocompatible, and that TAM-targeted delivery using the CHP nanogel would be feasible in the clinical setting (72-74).

Many efforts have been made to overcome tumor resistance to checkpoint inhibition (75-77). These studies have employed several strategies that involve combining checkpoint inhibitors with other reagents. For instance, Zamarin *et al.* reported that in immune-resistant B16 melanoma-bearing mice, specific T cell-inducing and therapeutic effects of anti-CTLA-4 antibody and oncolytic Newcastle disease virus (NDV) were greater than those with NDV alone (77). In contrast, our combination immunotherapy eradicates checkpoint inhibition-resistant tumors without the use of checkpoint inhibitors. The two therapies differ in their dependency on checkpoint inhibition, which

can be caused by the differential expression of checkpoint molecules on $CD8^+$ T cells, a main effector of tumor killing. B16 melanoma cells killed by NDV likely secrete highly immunogenic antigens, and T cells recognizing these antigens express PD-1 and CTLA-4 (38). In contrast, the DUC18 $CD8^+$ T cells used for adoptive transfer in our study did not express checkpoint molecules because they were naïve. Although further elucidation is necessary, to our knowledge, the current work successfully identified a novel combination immunotherapy that can cure checkpoint inhibition-resistant tumors without the use of checkpoint inhibitors.

To fully understand the mode of action of our combination immunotherapy, further analysis is required, for example, studies to identify the specific population of TAMs that play a vital role in this immunotherapy. Moreover, we could not have investigated whether this effect occurred in other tumors with low immunogenicity because we could not identify another tumor model similar to CMS5a fibrosarcoma in terms of low immunogenicity and checkpoint inhibition resistance. An analysis of human tumor samples is also important to clarify the relationship between inactive TAMs and the sensitivity to checkpoint inhibition. Nevertheless, our TAM-targeted combination immunotherapy addresses an important issue in current oncology, eradicating tumors that are completely resistant to checkpoint inhibition and providing a new opportunity to treat checkpoint inhibition-resistant human tumors.

Methods

Antibodies and other reagents. Fluorescently labeled monoclonal antibodies (mAbs) were purchased from Biolegend. They included anti-CD8 (clone 53-6.7), anti-Ly6C (clone HK1.4), anti-CD4 (clone RM4-5), anti-CD45RB/B220 (clone RM4-5), anti-CD11b (clone M1/70), anti-CD11c (clone N418), anti-F4/80 (clone BM8), anti-CD80 (clone 16-10A1), anti-CD86 (clone GL-1), anti-CD274 (clone 10F.9G2), anti-CD40 (clone 3/23), anti-I-A/I-E (clone M5/114), anti-KLRG1 (clone 2F1/KLRG1), anti-Tim3 (clone RMT3-23), anti-CD45 (clone 30-F11), anti-PD-1 (clone 29F.1A12), anti-IFN-γ (clone XMG1.2), anti-CD16/32 (clone 2.4G2), anti-Gr-1 (clone RB6-8C5), anti-T-bet (clone 4B10), Purified Rat IgG2a, κ Isotype Ctrl Antibody (clone RTK2758), Purified Rat IgG2b, κ Isotype Ctrl Antibody (clone RTK4530) and Mouse IgG2b, κ Isotype Ctrl Antibody (clone MPC11). Anti-mouse PD-1 (clone RMP1–14), anti-mouse CTLA-4 (clone 9D9) and anti-mouse GITR (clone DTA-1) mAbs were produced from hybridomas and purified using a protein G column. CpG ODN 1668 (5′-TCCATGACGTTCCTGATGCT-3′) was synthesized by Hokkaido System Science, Japan. Chemically synthesized long peptide antigens (LPAs) were obtained from Bio-Synthesis, Inc. Clodronate liposomes and control liposomes were purchased from FormuMax Scientific.

Fabrication of CHP nanogel and LPA complex. CHP powder was provided by Nippon Oil and Fat, Japan. The LPA consisting of 38 amino acid residues (SNPARYEFLYYYYYYQYIHSANVLYYYYYYRGPESRLL) contained three $CD8^+$ T cell epitopes, including MAGE-A4 p265-273 (SNPARYEFL) (48), 9m (QYIHSANVL) (51), and NY-ESO-1 p81-88 (RGPESRLL) (46), and another LPA consisting of 38 amino acid residues (SVYDFFVWLYYYYYYTWHRYHLLYYYYYYEGSRNQDWL) contained three $CD8^+$ T cell epitopes, including TRP2 p180-188 (SVYDFFVWL), TRP1 p222-229 (TWHRYHLL), and gp100 p25-33 (EGSRNQDWL); these LPAs were synthesized by Bio-synthesis, Inc. Oligotyrosine (YYYYYY) was included for efficient antigen processing. For analysis of antigen incorporation, the

LPA was labeled with FAM. CHP and LPA were dissolved in phosphate-buffered saline (PBS) containing 6 M urea and dimethyl sulfoxide, respectively. Both solutions were combined and gently mixed at 4°C, followed by dialysis against PBS to facilitate the formation of a complex between LPA and CHP by removing urea. The obtained CHP:LPA nanogel complex solution was stored at 4°C until use.

Mice. Female BALB/c and BALB/c nu/nu mice were obtained from SLC Japan and used at 6–12 weeks of age. DUC18 mice, transgenic for TCRα/β-reactive with a Kd-restricted 9m epitope, were established as previously described (61). DUC18 mice and CD90.1-congenic mice were mated, and DUC18/CD90.1 mice were obtained. Mice on a BALB/c background deficient in IFN-γ (IFN-γ -/-) were purchased from Taconic. All mice were maintained at the Animal Center of Mie University. The experimental protocols were approved by the Ethics Review Committee for Animal Experimentation of the university.

Tumors. CMS5a is a subclone derived from CMS5 that expresses the mutated ERK2 antigen containing 9m epitope. CMS5a/NY stably expresses the human cancer/testis antigen NY-ESO-1 (46). The colon epithelial tumor cell line CT26 (43, 44) was purchased from the American Type Culture Collection. CT26, CMS7 (45), CMS5a, and CMS5a/NY were cultured in RPMI1640 medium containing 10% fetal bovine serum (FBS). The melanoma tumor cell line B16 was purchased from the American Type Culture Collection. B16 cells were cultured in DMEM containing 10% FBS. Mice were inoculated subcutaneously in the hind flank with 1×10^6 cells of each tumor cell line and monitored three times a week. Tumor volume was calculated using the following formula: tumor volume = $0.5 \times$ length (mm) $\times$ [width (mm)]^2.

Administration of CHP:LPA complex, TLR agonist, and DUC18 CD8$^+$ T cells. To deplete macrophages, clodronate liposome solution (200 μl/mouse) was intravenously injected into mice 24 h prior to immunization. A CHP:LPA complex (50 μg LPA/mouse) was intravenously injected into

mice with or without CpG ODN (50 μg/mouse). One day after immunization, 2×10^6 $CD8^+$ T cells prepared from DUC18 mice were infused.

Flow cytometric analysis of immune cells. Cell suspensions prepared from tumor, spleen, and other tissues were stained for surface markers using mAbs at appropriate concentrations in PBS containing 2% FBS for 15 min at 4°C and analyzed on a FACSCanto II system (BD Biosciences). For intracellular cytokine staining, draining lymph node cells were incubated with the antigen peptide for 1 h at 37°C and then incubated for an additional 6 h with GolgiPlug (BD Biosciences). These cells were stained for surface markers. After permeabilization and fixation using a Cytofix/Cytoperm Kit (BD Biosciences), cells were stained with antibodies. After washing, cells were analyzed on a FACSCanto II using FlowJo software (Tree Star).

Reverse transcription quantitative polymerase chain reaction (RT-qPCR). Total RNA from cultured cells was reverse-transcribed to first-strand cDNA (cDNA) using a QuantiTect Reverse Transcription Kit (Qiagen). Quantitative PCR was performed using a StepOnePlus (Applied Biosystems, Carlsbad, CA, USA) according to the manufacturer's protocol. The primers and probe of CXCL9 were selected from the ABI TaqMan Gene Expression Assay catalog. *CXCL9* expression was normalized to that of *GAPDH*. Fold change was determined by the ΔΔCt method. Each experiment was performed in triplicate.

Tracking of injected antigen. A fluorescently labeled complex of CHP nanogel and LPA was intravenously or subcutaneously injected into tumor-bearing mice. The inguinal lymph node or tumor was harvested 16 h after the injection, homogenized, and filtered through a nylon mesh. The obtained cell suspension was analyzed by using flow cytometry for incorporation of labeled CHP or LPA and expression of CD45, CD11b, CD11c, F4/80, CD8, CD4, and B220.

Ex vivo antigen presentation. Antigen presentation by TAMs was evaluated ex vivo by measuring antigen-specific proliferation of $CD8^+$ T cells. CHP:LPA and CpG ODN were first

intravenously injected into tumor-bearing mice. The tumor was resected 18 h after injection. To isolate TAMs, the total cell suspension prepared from the tumor was mixed with anti-CD11b microbeads (Miltenyi Biotec) and separated by positive selection on a magnetic bead column. $CD11b^+$ cells were then stained with APC-labelled anti-Gr-1, PE-labeled anti-CD11b, PerCP-Cy5.5-labeled Ly6C, PE/Cy7-labelled F4/80, and APC/Cy7-labeled anti-CD45 mAbs, and sorted using a FACSAria (BD Biosciences). To isolate DCs, the total cell suspension prepared from the lymph node was mixed with anti-CD11c microbeads (Miltenyi Biotec) and separated by positive selection on a magnetic bead column. Isolated cells were co-cultured with 2.5×10^5 DUC18 T cells pre-labeled with a CFSE dye for 72 h. T cell proliferation was determined by quantifying CFSE dilution on a FACSCanto II system (BD Biosciences). IFN-γ production in the culture medium at 72 h was quantified using a mouse IFN-γ ELISA kit (BD Bioscience).

In vitro generation of mouse bone marrow-derived macrophages. Bone marrow cells were isolated from femurs of 7–10-week-old mice. Cells were cultured in 20 ng/ml M-CSF (Peprotech) in RPMI 1640 containing 10% FBS. After 7 days, macrophages were stimulated with 10 μg/ml CpG ODN for 12 h and pulsed with 10 μg/ml 9m peptide (QYIHSANVL) for 1 h.

Immunohistochemistry. Cryosections were prepared from tumors collected at 16 h after infusion of DUC18 $CD8^+$ T cells. OCT-embedded cryosections were stained with fluorescent dye-conjugated anti-PD-1, anti-PD-L1 or anti-MHC class II mAbs and observed under fluorescent microscopy (BX53, Olympus).

Microarray analysis of tumors. RNA was extracted from tumors or TAMs collected on day 7, and RNA quality was assessed using spectrophotometry and an Agilent Bioanalyzer 2100 (Agilent Technologies). Total RNA was amplified and labeled using the Ovation Pico WTA System and Encore Biotin Module (NuGEN). Prepared cDNA was hybridized to Affymetrix GeneChip Mouse Genome 430 2.0 arrays and scanned using a GeneChip Scanner 3000 7G (Affymetrix). Microarray

data are available in the DNA Data Bank of Japan (DDBJ, http://trace.ddbj.nig.ac.jp/DRASearch/) under accession no. E-GEAD-289 or E-GEAD-290.

Measurement of neoepitope-specific CD8$^+$ T cell responses. DNA and total RNA were extracted from in vitro cultured CT26, CMS7, and CMS5a cells. DNA was also extracted from the tails of BALB/c mice. Exome capture was performed using the SureSelectXT Mouse Exon Kit (Agilent Technologies). Exome capture libraries were then sequenced by Riken Genesis Co, Ltd., Japan on a HiSeq 2000 (Illumina) using an Illumina V3 Kit, resulting in 20 million (2 × 150 bp) exome reads from each library. RNA samples were used to generate RNA-seq libraries. RNA sequencing was performed by Hokkaido System Science Co., Ltd. on a HiSeq 2000, resulting in 30 million (2 × 100 bp) RNA fragments from each library.

Whole exome sequence reads were aligned to the mm9 reference sequence using the Burrows-Wheeler Aligner (BWA) (78). Somatic single nucleotide variants (SNVs) were detected using Fisher's exact test to compare read counts of normal and tumor samples. Variants with $p < 10^{-10}$ were considered statistically significant. From the identified SNVs, we extracted only non-synonymous SNVs. We also aligned the RNA-seq reads to the mm9 genome with Tophat using the Bowtie aligner (79). We next confirmed that RNAs carrying the detected SNVs were actually transcribed using the RNA-seq data. Among the aligned RNA sequence reads, candidate variants in the whole exome sequence were compared using Fisher's exact test. Variants with $p < 10^{-10}$ were considered to be transcribed SNVs. Whole exosome sequence data and RNA-seq data are available in the DDBJ under accession no. E-GEAD-291 or E-GEAD-292.

To prepare potential tumor-specific epitopes able to bind to murine MHC class I, we used IEDB Analysis Resource (http://www.iedb.org/). All candidate epitopes (8 to 10-mers) containing missense mutations were analyzed for their binding affinities to either H-2Kd, H-2Dd, or H-2Ld molecule based on the IEDB recommended method (consensus) consisting of the artificial neural

network (ANN), the stabilized matrix method (SMM), and the scoring matrices derived from combinatorial peptide libraries (Comblib_Sidney2008) algorithms (80). We prepared 61, 57, and 62 different candidate neoepitopes for CT26, CMS7, and CMS5a, respectively, based on those with a percentile rank ≤ 0.6 (Supplemental Tables 1−3).

Measurement of cytokines and chemokines in tumors. Tumors were harvested from CMS5a tumor-bearing mice, immediately frozen in liquid N_2, and store at -80°C. The tumors were then subjected to preparation of tumor lysate using Bio-Plex Cell Lysis Kit (Bio-Rad Laboratories) according to manufacturer's instruction. Protein concentration of tumor lysate was determined by using DC Protein Assay Kit (Bio-Rad Laboratories). The concentration of cytokines and chemokines was measured by using Bio-Plex Pro Mouse Cytokine GI 23-Plex and GII 9-Plex Panels (Bio-Rad Laboratories).

Retrovirus infection. Whole spleen cells (1.5×10^7 cells/5 mL) from BALB/c mice were stimulated with immobilized anti-CD3 (1 μg/mL; 145-2C11) and soluble anti-CD28 (1 μg/mL; 37.51). One day after stimulation, 5×10^5 cells were transduced with the viral vector encoding TCRs against the AH-1 using the RetroNectin-bound virus infection method (81). On day 5, the cells were harvested and used for experiments. Recombinant human IL-2 (Novartis) at 60 IU/mL was added during culturing.

Dynamic light-scattering (DLS). DLS measurement was performed using a Zetasizer Nano ZS (Malvern Instruments, Ltd.) at 633 nm and a 173° detection angle at 25°C. The measured auto-correlation function was analyzed using the cumulant method. The hydrodynamic diameter (DH) of the samples was calculated from the Stokes-Einstein equation. The ζ-potential of the CHP:LPA complex was also measured using the Zetasizer Nano ZS at a 90° detection angle at 25°C in PBS.

Transmission electron microscopy (TEM). The sample was applied to a carbon-coated grid, and the grid was stained with TI blue (Nisshin EM, Japan), dried, and subjected to TEM (HT7700, Hitachi) at an accelerating voltage of 100 kV.

Hematoxylin and eosin staining. Paraffin-embedded sections of mouse tissues fixed with 10% buffered formalin were subjected to H&E staining.

Statistical analysis. Data obtained in the in vivo tumor growth experiments were processed using Mann-Whitney U test or the Steel-Dwass test. The remaining data were analyzed using 2-tailed Student's *t*-test, Dunnett test, or a two-factor factorial ANOVA followed by Tukey-Kramer post hoc analysis. Comparisons where $p < 0.05$ were considered significant.

Study approval. All animal studies were performed with the approval of the IACUC of Mie University and the IACUC of University of Shizuoka.

Data availability. All data in this manuscript are available from the authors on request.

Author contributions

DM, NH, and HS designed the study and wrote, reviewed, and revised the manuscript; DM, TH, KF, IT, YM and KO performed animal and immunological experiments; NS and YT performed immunohistochemical analysis; NH and TH designed and prepared CHP:LPA; DM, NS, TH, and NH analyzed and interpreted data; DM, RY, MK, and SI performed bioinformatics analysis on neoantigens; TY and MG performed chemical analysis of CHP:LPA; HY and SS provided key materials; KA, AA, HI and SM provided key discussions.

Acknowledgments

We thank Dr. T. Takahashi for helpful discussion and Dr. L. Wang, and K. Mori for technical assistance. This study was partially supported by Japan Society for the Promotion of Science

KAKENHI (Grant Number 15K18443) and Exploratory Research for Advanced Technology of the Japan Science and Technology Agency (JST ERATO).

References

1. Mellman I, Coukos G, and Dranoff G. Cancer immunotherapy comes of age. *Nature.* 2011;480(7378):480-489.
2. Wolchok JD, et al. Nivolumab plus ipilimumab in advanced melanoma. *N Engl J Med.* 2013;369(2):122-133.
3. Callahan MK, and Wolchok JD. At the bedside: CTLA-4- and PD-1-blocking antibodies in cancer immunotherapy. *J Leukoc Biol.* 2013;94(1):41-53.
4. Topalian SL, et al. Survival, durable tumor remission, and long-term safety in patients with advanced melanoma receiving nivolumab. *J Clin Oncol.* 2014;32(10):1020-1030.
5. Gubin MM, et al. Checkpoint blockade cancer immunotherapy targets tumour-specific mutant antigens. *Nature.* 2014;515(7528):577-581.
6. Zou W, Wolchok JD, and Chen L. PD-L1 (B7-H1) and PD-1 pathway blockade for cancer therapy: Mechanisms, response biomarkers, and combinations. *Sci Transl Med.* 2016;8(328):328rv324.
7. Iwai Y, Hamanishi J, Chamoto K, and Honjo T. Cancer immunotherapies targeting the PD-1 signaling pathway. *J Biomed Sci.* 2017;24(1):26.
8. Herbst RS, et al. Predictive correlates of response to the anti-PD-L1 antibody MPDL3280A in cancer patients. *Nature.* 2014;515(7528):563-567.
9. Powles T, et al. MPDL3280A (anti-PD-L1) treatment leads to clinical activity in metastatic bladder cancer. *Nature.* 2014;515(7528):558-562.
10. Rizvi NA, et al. Cancer immunology. Mutational landscape determines sensitivity to PD-1 blockade in non-small cell lung cancer. *Science.* 2015;348(6230):124-128.
11. Taube JM, et al. Colocalization of inflammatory response with B7-h1 expression in human melanocytic lesions supports an adaptive resistance mechanism of immune escape. *Sci Transl Med.* 2012;4(127):127ra137.
12. Tumeh PC, et al. PD-1 blockade induces responses by inhibiting adaptive immune resistance. *Nature.* 2014;515(7528):568-571.
13. Larkin J, et al. Combined Nivolumab and Ipilimumab or Monotherapy in Untreated Melanoma. *N Engl J Med.* 2015;373(1):23-34.
14. Peng W, et al. Loss of PTEN Promotes Resistance to T Cell-Mediated Immunotherapy. *Cancer Discov.* 2016;6(2):202-216.
15. Manguso RT, et al. In vivo CRISPR screening identifies Ptpn2 as a cancer immunotherapy target. *Nature.* 2017;547(7664):413-418.
16. Spranger S, Bao R, and Gajewski TF. Melanoma-intrinsic beta-catenin signalling prevents anti-tumour immunity. *Nature.* 2015;523(7559):231-235.
17. Sivan A, et al. Commensal Bifidobacterium promotes antitumor immunity and facilitates anti-PD-L1 efficacy. *Science.* 2015;350(6264):1084-1089.
18. Tran E, et al. Immunogenicity of somatic mutations in human gastrointestinal cancers. *Science.* 2015;350(6266):1387-1390.
19. Franklin RA, et al. The cellular and molecular origin of tumor-associated macrophages. *Science.* 2014;344(6186):921-925.
20. Lavin Y, et al. Tissue-resident macrophage enhancer landscapes are shaped by the local microenvironment. *Cell.* 2014;159(6):1312-1326.
21. Colegio OR, et al. Functional polarization of tumour-associated macrophages by tumour-derived lactic acid. *Nature.* 2014;513(7519):559-563.
22. Laoui D, et al. Tumor hypoxia does not drive differentiation of tumor-associated macrophages but rather fine-tunes the M2-like macrophage population. *Cancer Res.* 2014;74(1):24-30.
23. Ruffell B, et al. Macrophage IL-10 blocks $CD8^+$ T cell-dependent responses to chemotherapy by suppressing IL-12 expression in intratumoral dendritic cells. *Cancer Cell.* 2014;26(5):623-637.
24. Doedens AL, et al. Macrophage expression of hypoxia-inducible factor-1 alpha suppresses T-cell function and promotes tumor progression. *Cancer Res.* 2010;70(19):7465-7475.

25. Hesse M, et al. Differential regulation of nitric oxide synthase-2 and arginase-1 by type 1/type 2 cytokines in vivo: granulomatous pathology is shaped by the pattern of L-arginine metabolism. *J Immunol.* 2001;167(11):6533-6544.
26. Gao J, et al. VISTA is an inhibitory immune checkpoint that is increased after ipilimumab therapy in patients with prostate cancer. *Nat Med.* 2017;23(5):551-555.
27. DeNardo DG, et al. Leukocyte complexity predicts breast cancer survival and functionally regulates response to chemotherapy. *Cancer Discov.* 2011;1(1):54-67.
28. Germano G, et al. Role of macrophage targeting in the antitumor activity of trabectedin. *Cancer Cell.* 2013;23(2):249-262.
29. Predina J, et al. Changes in the local tumor microenvironment in recurrent cancers may explain the failure of vaccines after surgery. *Proc Natl Acad Sci U S A.* 2013;110(5):E415-424.
30. Kaneda MM, et al. PI3Kgamma is a molecular switch that controls immune suppression. *Nature.* 2016;539(7629):437-442.
31. Kitano S, et al. HER2-specific T-cell immune responses in patients vaccinated with truncated HER2 protein complexed with nanogels of cholesteryl pullulan. *Clin Cancer Res.* 2006;12(24):7397-7405.
32. Gu XG, et al. A novel hydrophobized polysaccharide/oncoprotein complex vaccine induces in vitro and in vivo cellular and humoral immune responses against HER2-expressing murine sarcomas. *Cancer Res.* 1998;58(15):3385-3390.
33. Akiyoshi K, et al. Self-assembled hydrogel nanoparticle of cholesterol-bearing pullulan as a carrier of protein drugs: complexation and stabilization of insulin. *J Control Release.* 1998;54(3):313-320.
34. Sasaki Y, and Akiyoshi K. Nanogel engineering for new nanobiomaterials: from chaperoning engineering to biomedical applications. *Chem Rec.* 2010;10(6):366-376.
35. Tahara Y, and Akiyoshi K. Current advances in self-assembled nanogel delivery systems for immunotherapy. *Adv Drug Deliv Rev.* 2015;95:65-76.
36. Muraoka D, et al. Nanogel-based immunologically stealth vaccine targets macrophages in the medulla of lymph node and induces potent antitumor immunity. *ACS Nano.* 2014;8(9):9209-9218.
37. Lu L, Xu X, Zhang B, Zhang R, Ji H, and Wang X. Combined PD-1 blockade and GITR triggering induce a potent antitumor immunity in murine cancer models and synergizes with chemotherapeutic drugs. *J Transl Med.* 2014;12:36.
38. Curran MA, Montalvo W, Yagita H, and Allison JP. PD-1 and CTLA-4 combination blockade expands infiltrating T cells and reduces regulatory T and myeloid cells within B16 melanoma tumors. *Proc Natl Acad Sci U S A.* 2010;107(9):4275-4280.
39. Krummel MF, and Allison JP. CTLA-4 engagement inhibits IL-2 accumulation and cell cycle progression upon activation of resting T cells. *J Exp Med.* 1996;183(6):2533-2540.
40. Simpson TR, et al. Fc-dependent depletion of tumor-infiltrating regulatory T cells co-defines the efficacy of anti-CTLA-4 therapy against melanoma. *J Exp Med.* 2013;210(9):1695-1710.
41. Ko K, et al. Treatment of advanced tumors with agonistic anti-GITR mAb and its effects on tumor-infiltrating $Foxp3^{+}CD25^{+}CD4^{+}$ regulatory T cells. *J Exp Med.* 2005;202(7):885-891.
42. Bulliard Y, et al. Activating Fc gamma receptors contribute to the antitumor activities of immunoregulatory receptor-targeting antibodies. *J Exp Med.* 2013;210(9):1685-1693.
43. Corbett TH, Griswold DP, Jr., Roberts BJ, Peckham JC, and Schabel FM, Jr. Tumor induction relationships in development of transplantable cancers of the colon in mice for chemotherapy assays, with a note on carcinogen structure. *Cancer Res.* 1975;35(9):2434-2439.
44. Griswold DP, and Corbett TH. A colon tumor model for anticancer agent evaluation. *Cancer.* 1975;36(6 Suppl):2441-2444.
45. DeLeo AB, Shiku H, Takahashi T, John M, and Old LJ. Cell surface antigens of chemically induced sarcomas of the mouse. I. Murine leukemia virus-related antigens and alloantigens on cultured fibroblasts and sarcoma cells: description of a unique antigen on BALB/c Meth A sarcoma. *J Exp Med.* 1977;146(3):720-734.
46. Muraoka D, et al. Peptide vaccine induces enhanced tumor growth associated with apoptosis induction in $CD8^{+}$ T cells. *J Immunol.* 2010;185(6):3768-3776.

47. Gnjatic S, et al. NY-ESO-1: review of an immunogenic tumor antigen. *Adv Cancer Res.* 2006;95:1-30.
48. Muraoka D, et al. Establishment of animal models to analyze the kinetics and distribution of human tumor antigen-specific $CD8^+$ T cells. *Vaccine.* 2013;31(17):2110-2118.
49. Fujii K, et al. Identification of an immunogenic neo-epitope encoded by mouse sarcoma using CXCR3 ligand mRNAs as sensors. *Oncoimmunology.* 2017;6(5):e1306617.
50. Huang AY, et al. The immunodominant major histocompatibility complex class I-restricted antigen of a murine colon tumor derives from an endogenous retroviral gene product. *Proc Natl Acad Sci U S A.* 1996;93(18):9730-9735.
51. Ikeda H, et al. Mutated mitogen-activated protein kinase: a tumor rejection antigen of mouse sarcoma. *Proc Natl Acad Sci U S A.* 1997;94(12):6375-6379.
52. Duan F, et al. Genomic and bioinformatic profiling of mutational neoepitopes reveals new rules to predict anticancer immunogenicity. *J Exp Med.* 2014;211(11):2231-2248.
53. Sakuishi K, Apetoh L, Sullivan JM, Blazar BR, Kuchroo VK, and Anderson AC. Targeting Tim-3 and PD-1 pathways to reverse T cell exhaustion and restore anti-tumor immunity. *J Exp Med.* 2010;207(10):2187-2194.
54. Eikawa S, Nishida M, Mizukami S, Yamazaki C, Nakayama E, and Udono H. Immune-mediated antitumor effect by type 2 diabetes drug, metformin. *Proc Natl Acad Sci U S A.* 2015;112(6):1809-1814.
55. Joshi NS, et al. Inflammation directs memory precursor and short-lived effector $CD8^+$ T cell fates via the graded expression of T-bet transcription factor. *Immunity.* 2007;27(2):281-295.
56. Oosterwegel MA, Greenwald RJ, Mandelbrot DA, Lorsbach RB, and Sharpe AH. CTLA-4 and T cell activation. *Curr Opin Immunol.* 1999;11(3):294-300.
57. Nocentini G, and Riccardi C. GITR: a modulator of immune response and inflammation. *Adv Exp Med Biol.* 2009;647:156-173.
58. Litvak V, et al. Function of C/EBPdelta in a regulatory circuit that discriminates between transient and persistent TLR4-induced signals. *Nat Immunol.* 2009;10(4):437-443.
59. Kurozumi K, et al. Effect of tumor microenvironment modulation on the efficacy of oncolytic virus therapy. *J Natl Cancer Inst.* 2007;99(23):1768-1781.
60. Liberzon A, Birger C, Thorvaldsdottir H, Ghandi M, Mesirov JP, and Tamayo P. The Molecular Signatures Database (MSigDB) hallmark gene set collection. *Cell Syst.* 2015;1(6):417-425.
61. Hanson HL, et al. Eradication of established tumors by $CD8^+$ T cell adoptive immunotherapy. *Immunity.* 2000;13(2):265-276.
62. Kerkar SP, et al. IL-12 triggers a programmatic change in dysfunctional myeloid-derived cells within mouse tumors. *J Clin Invest.* 2011;121(12):4746-4757.
63. Bae YH, and Park K. Targeted drug delivery to tumors: myths, reality and possibility. *J Control Release.* 2011;153(3):198-205.
64. Greish K. Enhanced permeability and retention (EPR) effect for anticancer nanomedicine drug targeting. *Methods Mol Biol.* 2010;624:25-37.
65. Matsumoto Y, et al. Vascular bursts enhance permeability of tumour blood vessels and improve nanoparticle delivery. *Nat Nanotechnol.* 2016;11(6):533-538.
66. Schliehe C, et al. CD8- dendritic cells and macrophages cross-present poly(D,L-lactate-co-glycolate) acid microsphere-encapsulated antigen in vivo. *J Immunol.* 2011;187(5):2112-2121.
67. Barral P, et al. $CD169^+$ macrophages present lipid antigens to mediate early activation of iNKT cells in lymph nodes. *Nat Immunol.* 2010;11(4):303-312.
68. Kao C, et al. Transcription factor T-bet represses expression of the inhibitory receptor PD-1 and sustains virus-specific $CD8^+$ T cell responses during chronic infection. *Nat Immunol.* 2011;12(7):663-671.
69. Kim WG, et al. Covalent Conjugation of Small-Molecule Adjuvants to Nanoparticles Induces Robust Cytotoxic T Cell Responses via DC Activation. *Bioconjug Chem.* 2016;27(9):2007-2013.

70. van der Sluis TC, et al. Therapeutic Peptide Vaccine-Induced CD8 T Cells Strongly Modulate Intratumoral Macrophages Required for Tumor Regression. *Cancer Immunol Res.* 2015;3(9):1042-1051.
71. Mills CD, Lenz LL, and Harris RA. A Breakthrough: Macrophage-Directed Cancer Immunotherapy. *Cancer Res.* 2016;76(3):513-516.
72. Miyauchi K, et al. Clinical relevance of antigen spreading pattern induced by CHP-MAGE-A4 cancer vaccination. *Immunotherapy.* 2016;8(5):527-540.
73. Kageyama S, et al. Dose-dependent effects of NY-ESO-1 protein vaccine complexed with cholesteryl pullulan (CHP-NY-ESO-1) on immune responses and survival benefits of esophageal cancer patients. *J Transl Med.* 2013;11:246.
74. Aoki M, et al. Antibody responses against NY-ESO-1 and HER2 antigens in patients vaccinated with combinations of cholesteryl pullulan (CHP)-NY-ESO-1 and CHP-HER2 with OK-432. *Vaccine.* 2009;27(49):6854-6861.
75. Kim K, et al. Eradication of metastatic mouse cancers resistant to immune checkpoint blockade by suppression of myeloid-derived cells. *Proc Natl Acad Sci U S A.* 2014;111(32):11774-11779.
76. Fu J, et al. STING agonist formulated cancer vaccines can cure established tumors resistant to PD-1 blockade. *Sci Transl Med.* 2015;7(283):283ra252.
77. Zamarin D, et al. Localized oncolytic virotherapy overcomes systemic tumor resistance to immune checkpoint blockade immunotherapy. *Sci Transl Med.* 2014;6(226):226ra232.
78. Li H, and Durbin R. Fast and accurate short read alignment with Burrows-Wheeler transform. *Bioinformatics.* 2009;25(14):1754-1760.
79. Trapnell C, Pachter L, and Salzberg SL. TopHat: discovering splice junctions with RNA-Seq. *Bioinformatics.* 2009;25(9):1105-1111.
80. Moutaftsi M, et al. A consensus epitope prediction approach identifies the breadth of murine T_{CD8+}-cell responses to vaccinia virus. *Nat Biotechnol.* 2006;24(7):817-819.
81. Wang L, et al. Efficient tumor regression by adoptively transferred CEA-specific CAR-T cells associated with symptoms of mild cytokine release syndrome. *Oncoimmunology.* 2016;5(9):e1211218.

Figures

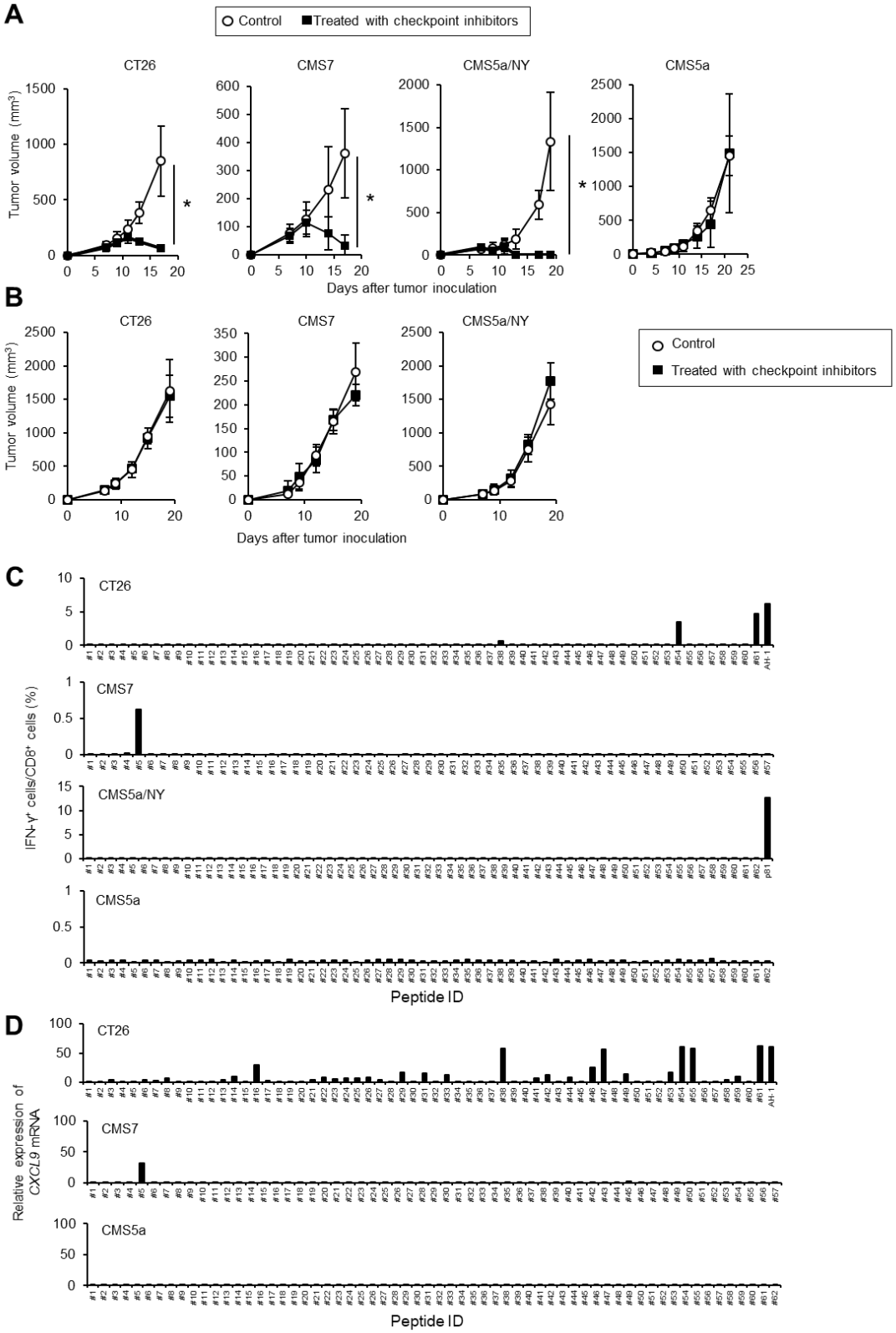
A
Control
Treated with checkpoint inhibitors
CT26
CMS7
CMS5a/NY
CMS5a
Tumor volume (mm3)
Days after tumor inoculation
B
Control
Treated with checkpoint inhibitors
C
IFN-γ+ cells/CD8+ cells (%)
Peptide ID
D
Relative expression of CXCL9 mRNA
Peptide ID

Figure 1. Murine fibrosarcoma CMS5a is highly refractory to checkpoint inhibition and lacks specific CD8$^+$ T cell response. (**A**) Murine tumor cell line CT26, CMS7, CMS5a/NY, or CMS5a was subcutaneously inoculated into BALB/c mice. Checkpoint inhibitors including anti-PD-1 (200 μg/mouse), anti-CTLA-4 (100 μg/mouse), and anti-GITR (200 μg/mouse) antibodies (n = 8 to 10 per group) or isotype control antibodies (n = 8 per group) were intraperitoneally injected on days 7, 9, and 11. (**B**) The experiment was performed in nude mice as described in **A**. (**C,D**) Induction of tumor-specific CD8$^+$ T cell response by checkpoint inhibition was evaluated. BALB/c mice bearing CT26, CMS7, CMS5a/NY, or CMS5a tumors were treated with checkpoint inhibitors. Seven days after the last administration, splenocytes were isolated and re-stimulated with peptides of predicted neoepitopes or known tumor antigens (AH-1 in CT26 and NY-ESO-1 p81 in CMS5a/NY). The frequency of stimulated CD8$^+$ T cells was quantified by (**C**) intracellular IFN-γ staining (four mice per group) or (**D**) the fold increase in *CXCL9* mRNA levels compared with DMSO. These experiments were repeated at least twice to four times with similar results. p-values were determined by Mann-Whitney U test. *, $p < 0.05$

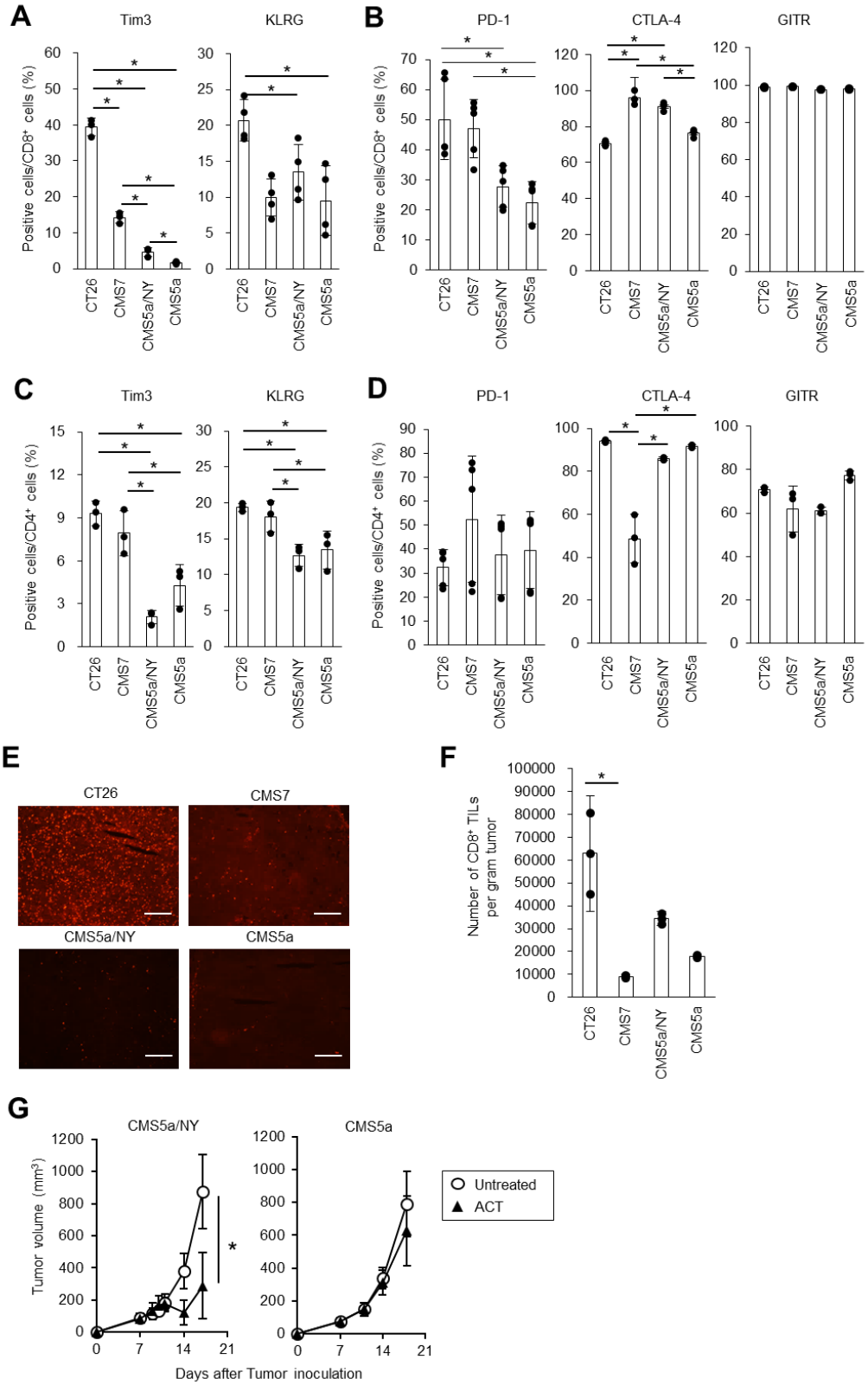
A
Tim3
KLRG
Positive cells/CD8+ cells (%)
B
PD-1
CTLA-4
GITR
Positive cells/CD8+ cells (%)
C
Tim3
KLRG
Positive cells/CD4+ cells (%)
D
PD-1
CTLA-4
GITR
Positive cells/CD4+ cells (%)
CT26
CMS7
CMS5a/NY
CMS5a
E
CT26
CMS7
CMS5a/NY
CMS5a
F
Number of CD8+ TILs per gram tumor
G
CMS5a/NY
CMS5a
Tumor volume (mm3)
Days after Tumor inoculation
Untreated
ACT

Figure 2. TIL activation and systemic T cell response do not correlate with sensitivity to checkpoint inhibition. (**A, B**) Expression of Tim3, KLRG, PD-1, CTLA-4 and GITR on $CD8^+$ TILs from indicated tumors was determined by flow cytometry 7 days after tumor inoculation (n = 3 or 4 per group). (**C, D**) The experiment was performed as in a but on $CD4^+$ TILs. p-values were determined by a two-factor factorial ANOVA followed by Tukey–Kramer post hoc analysis. *, $p < 0.05$. These experiments were repeated thrice with similar results. (**E**) PD-1 expression was also analyzed by immunohistochemistry. The scale bar represents 200 μm. (**F**) The number of $CD8^+$ TILs was quantified in each tumor (n = 3 per group). p-values were determined by a two-factor factorial ANOVA followed by Tukey–Kramer post hoc analysis. *, $p < 0.05$. These experiments were repeated twice with similar results. (**G**) $CD8^+$ T cells (2×10^6) isolated from DUC18 mice were infused to the CMS5a/NY or CMS5a-bearing mice on day 7, and the tumor size was monitored. Each group had 5 mice. p-values were determined by Mann-Whitney U test. *, $p < 0.05$. n.s., not significant. These experiments were repeated thrice with similar results.

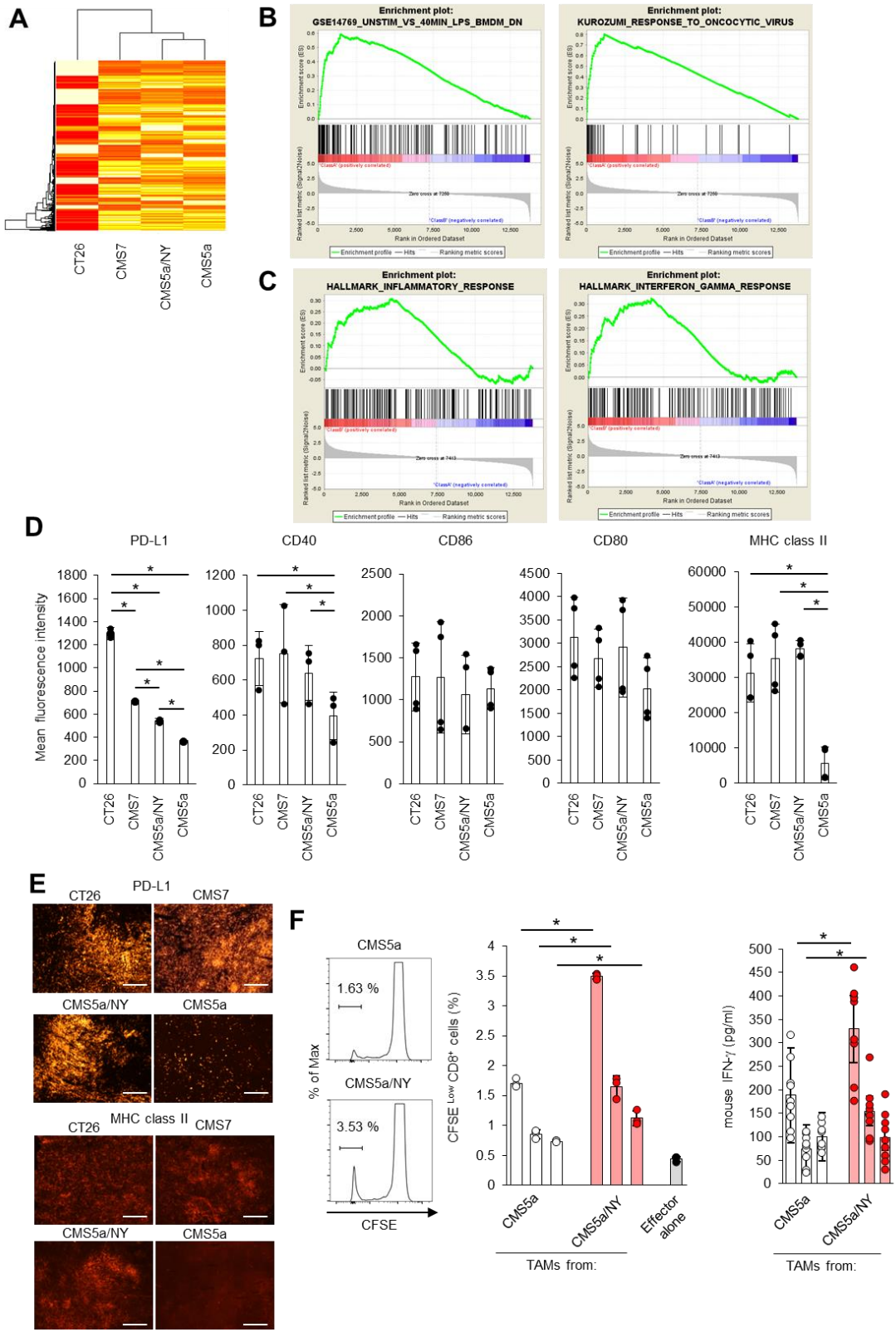
A
CT26
CMS7
CMS5a/NY
CMS5a
B
Enrichment plot:
GSE14769_UNSTIM_VS_40MIN_LPS_BMDM_DN
Enrichment plot:
KUROZUMI_RESPONSE_TO_ONCOCYTIC_VIRUS
C
Enrichment plot:
HALLMARK_INFLAMMATORY_RESPONSE
Enrichment plot:
HALLMARK_INTERFERON_GAMMA_RESPONSE
D
PD-L1
CD40
CD86
CD80
MHC class II
Mean fluorescence intensity
E
PD-L1
CT26
CMS7
CMS5a/NY
CMS5a
MHC class II
F
CMS5a
1.63 %
CMS5a/NY
3.53 %
% of Max
CFSE
CFSE Low CD8+ cells (%)
Effector alone
TAMs from:
mouse IFN-γ (pg/ml)

Figure 3. TAMs remain inactive in the resistant CMS5a tumor. (**A**) Tumor tissue from the CT26-, CMS7-, CMS5a/NY-, or CMS5a-bearing mice was collected 7 days after inoculation and subjected to microarray analysis. (**B**) Subsequent GSEA identified down regulation of two indicated gene sets in resistant CMS5a tumors. (**C**) TAMs from the CT26-, CMS7-, CMS5a/NY-, or CMS5a-bearing mice were collected and total RNA from these TAMs were subjected to microarray analysis. Subsequent GSEA identified downregulation of two indicated gene sets in TAMs from CMS5a. (**D**) TAMs were isolated from each tumor at 7 days after inoculation, and were tested for the expression of PD-L1, CD40, CD86, CD80, and MHC class II by flow cytometry (six tumors per group). p-values were determined by a two-factor factorial ANOVA followed by Tukey–Kramer post hoc analysis. *, $p < 0.05$. These experiments were repeated thrice with similar results. (**E**) PD-L1 and MHC class II expression was also analyzed by immunohistochemistry. The scale bar represents 200 μm. (**F**) TAMs isolated from the CMS5a-bearing mice on day 7 were co-cultured as antigen-presenting cells with 9m-specific DUC18 $CD8^+$ T cells as responder cells for 72 h. Antigen-dependent proliferation of DUC18 $CD8^+$ T cells and production of IFN-γ were measured by using a CFSE dilution assay (n = 3 or 4 per group) or ELISA (n = 8 or 9 per group) respectively. The histograms show representative data, and the numbers shown in histograms indicate the percentage of proliferating cells. p-values were determined by 2-tailed Student's t-test. The data are the mean ± SD. *, $p < 0.05$. These experiments were repeated twice with similar results.

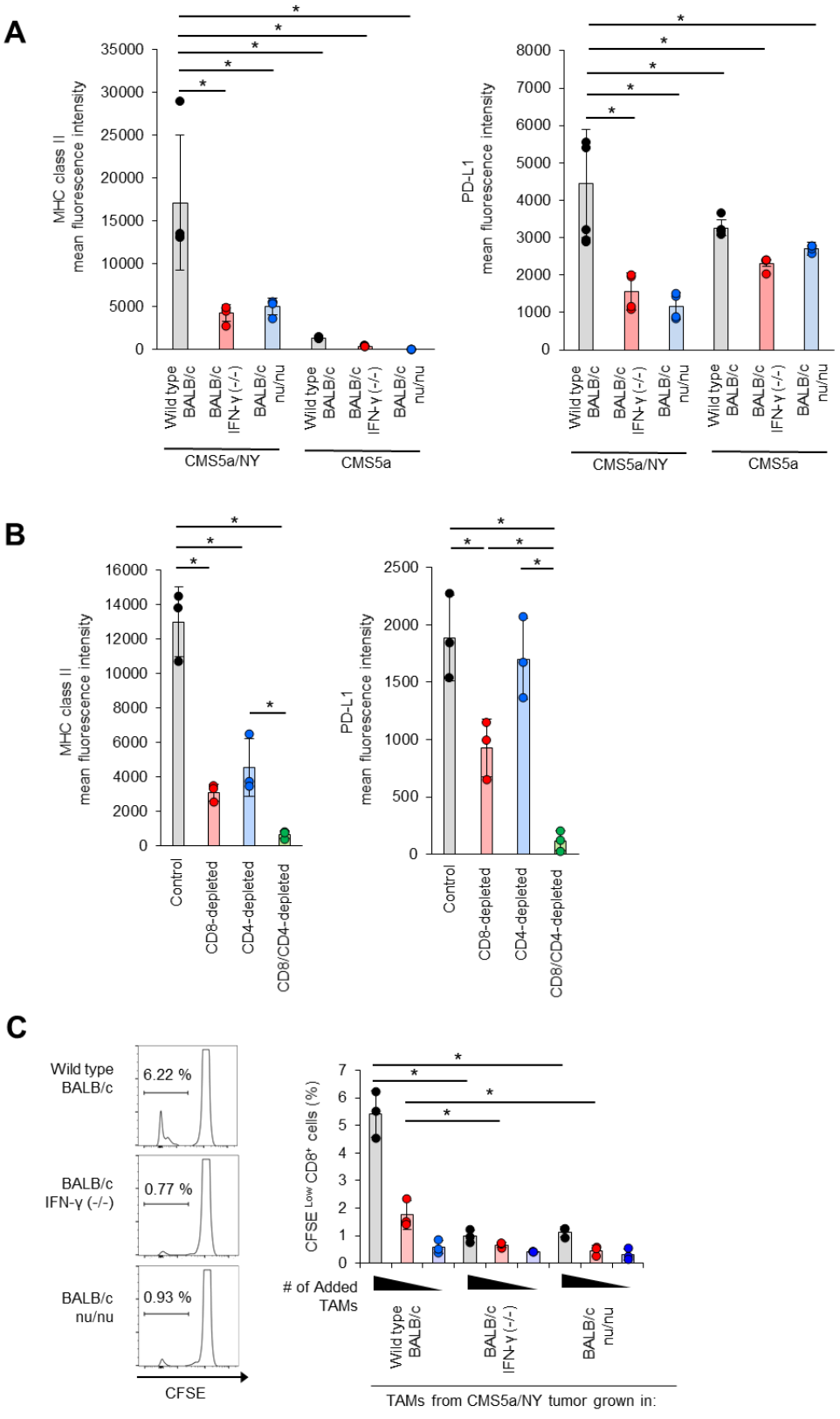
A
MHC class II
mean fluorescence intensity
PD-L1
mean fluorescence intensity
Wild type BALB/c
BALB/c IFN-γ (-/-)
BALB/c nu/nu
CMS5a/NY
CMS5a
B
MHC class II
mean fluorescence intensity
PD-L1
mean fluorescence intensity
Control
CD8-depleted
CD4-depleted
CD8/CD4-depleted
C
Wild type BALB/c
6.22 %
BALB/c IFN-γ (-/-)
0.77 %
BALB/c nu/nu
0.93 %
CFSE
CFSE Low CD8+ cells (%)
# of Added TAMs
TAMs from CMS5a/NY tumor grown in:

Figure 4. TAM activation in sensitive tumors is dependent on IFN-γ signaling and T cells. (**A**) CMS5a/NY or CMS5a cells were subcutaneously inoculated into wild type BALB/c mice (gray, n = 3), BALB/c IFN-γ (-/-) mice (blue, n = 3), or BALB/c nu/nu mice (red, n = 3). Seven days after inoculation, TAMs were isolated and analyzed for PD-L1 and MHC class II expression. The histograms show representative data. (**B**) The experiment was performed as described in a but in $CD8^+$ T cell- (red, n = 3), $CD4^+$ T cell- (blue, n = 3), or $CD8^+$ T cell/$CD4^+$ T cell-depleted (green, n = 3) mice. (**C**) TAMs were sorted from CMS5a/NY tumors grown in wild-type BALB/c mice (n = 3), BALB/c IFN-γ (-/-) mice (n = 3), or BALB/c nu/nu mice (n = 3), and were co-cultured as antigen-presenting cells (1, 0.25 or 0.125 $x10^5$ cells / well) with DUC18 $CD8^+$ T cells as responder cells for 72 h. Antigen-dependent proliferation of DUC18 $CD8^+$ T cells was measured using a CFSE dilution assay. The histograms show representative data, and the numbers shown in histograms indicate the percentage of proliferating $CD8^+$ T cells. Data are the mean ± SD. p-values were determined by a two-factor factorial ANOVA followed by Tukey–Kramer post hoc analysis. *, $p < 0.05$. These experiments were repeated at least two to four times with similar results.

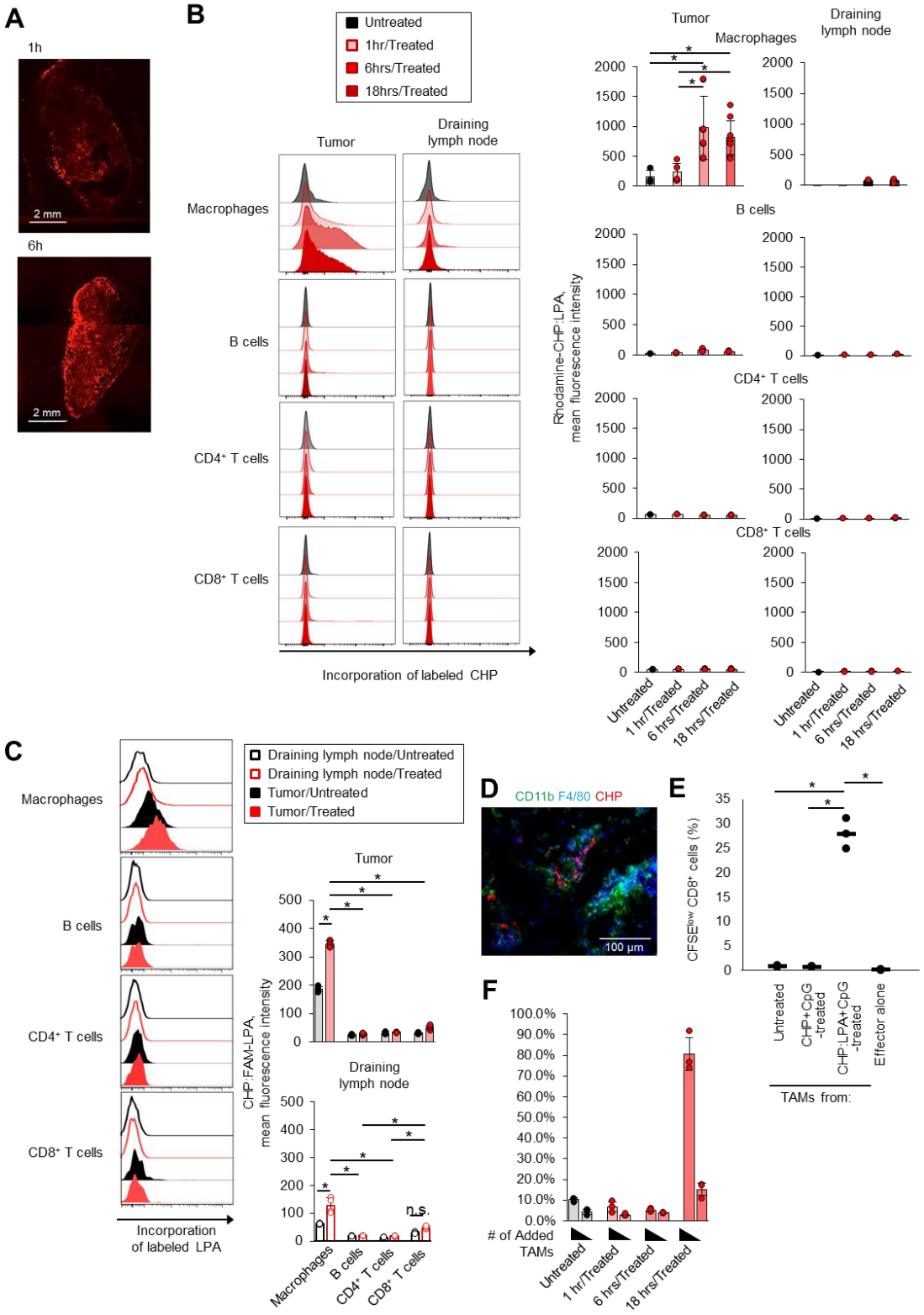
A
1h
2 mm
6h
2 mm
B
Untreated
1hr/Treated
6hrs/Treated
18hrs/Treated
Tumor
Draining lymph node
Macrophages
B cells
CD4⁺ T cells
CD8⁺ T cells
Incorporation of labeled CHP
Rhodamine-CHP:LPA, mean fluorescence intensity
Untreated
1 hr/Treated
6 hrs/Treated
18 hrs/Treated
C
Draining lymph node/Untreated
Draining lymph node/Treated
Tumor/Untreated
Tumor/Treated
Incorporation of labeled LPA
CHP:FAM-LPA, mean fluorescence intensity
n.s.
D
CD11b F4/80 CHP
100 µm
E
CFSE^low CD8⁺ cells (%)
Untreated
CHP+CpG -treated
CHP:LPA+CpG -treated
Effector alone
TAMs from:
F
# of Added TAMs

Figure 5. Targeted antigen delivery using CHP nanogel improves antigen presenting activity of TAMs. (**A**) CMS5a tumor-bearing BALB/c mice were intravenously injected with rhodamine-CHP:LPA, and 1 or 6 h later, tumors were removed. The distribution of rhodamine-CHP in the tumor was observed using confocal laser microscopy. (**B**) CMS5a tumor-bearing BALB/c mice were intravenously injected with rhodamine-CHP:LPA complex, and 1, 6, or 18 h later, immune cells including $CD11b^+F4/80^+$ macrophages, B cells, $CD8^+$ T cells, and $CD4^+$ T cells in the tumor or the tumor-draining lymph node were isolated (n = 4 per group). The uptake of labeled CHP:LPA in these cells was measured using flow cytometry. The histograms show the representative data for CHP:LPA incorporation. (**C**) CMS5a tumor-bearing BALB/c mice were intravenously injected with CHP:FAM-LPA complex, and 18 h later, the uptake of CHP:FAM-LPA in these cells was measured using flow cytometry (three mice per group). The histograms show representative data for CHP:LPA incorporation. p-values were determined by a two-factor factorial ANOVA followed by Tukey–Kramer post hoc analysis. *, $p < 0.05$. These experiments were repeated thrice with similar results. (**D**) CMS5a tumor-bearing BALB/c mice were treated as same in **A**, and 6 h later, cryosections of tumor was prepared. Incorporation of rhodamine-CHP:LPA into $CD11b^+F4/80^+$ TAMs was observed by immunohistochemistry. (**E, F**) The complex of CHP with 9m-containing LPA (50 μg) was intravenously injected with CpG ODN (50 μg) into BALB/c mice. After 1, 6 or 18 h, TAMs were isolated and co-cultured as antigen-presenting cells with DUC18 $CD8^+$ T cells as responder cells for 72 h. Antigen-dependent proliferation of DUC18 $CD8^+$ T cells was measured using a CFSE dilution assay (n = 3 per group). The histograms show the representative data, and the numbers shown in histograms indicate the percentage of proliferating $CD8^+$ T cells. Data are the mean ± SD. p-values were

determined by a two-factor factorial ANOVA followed by Tukey–Kramer post hoc analysis. *, $p < 0.05$. These experiments were repeated twice with similar results.

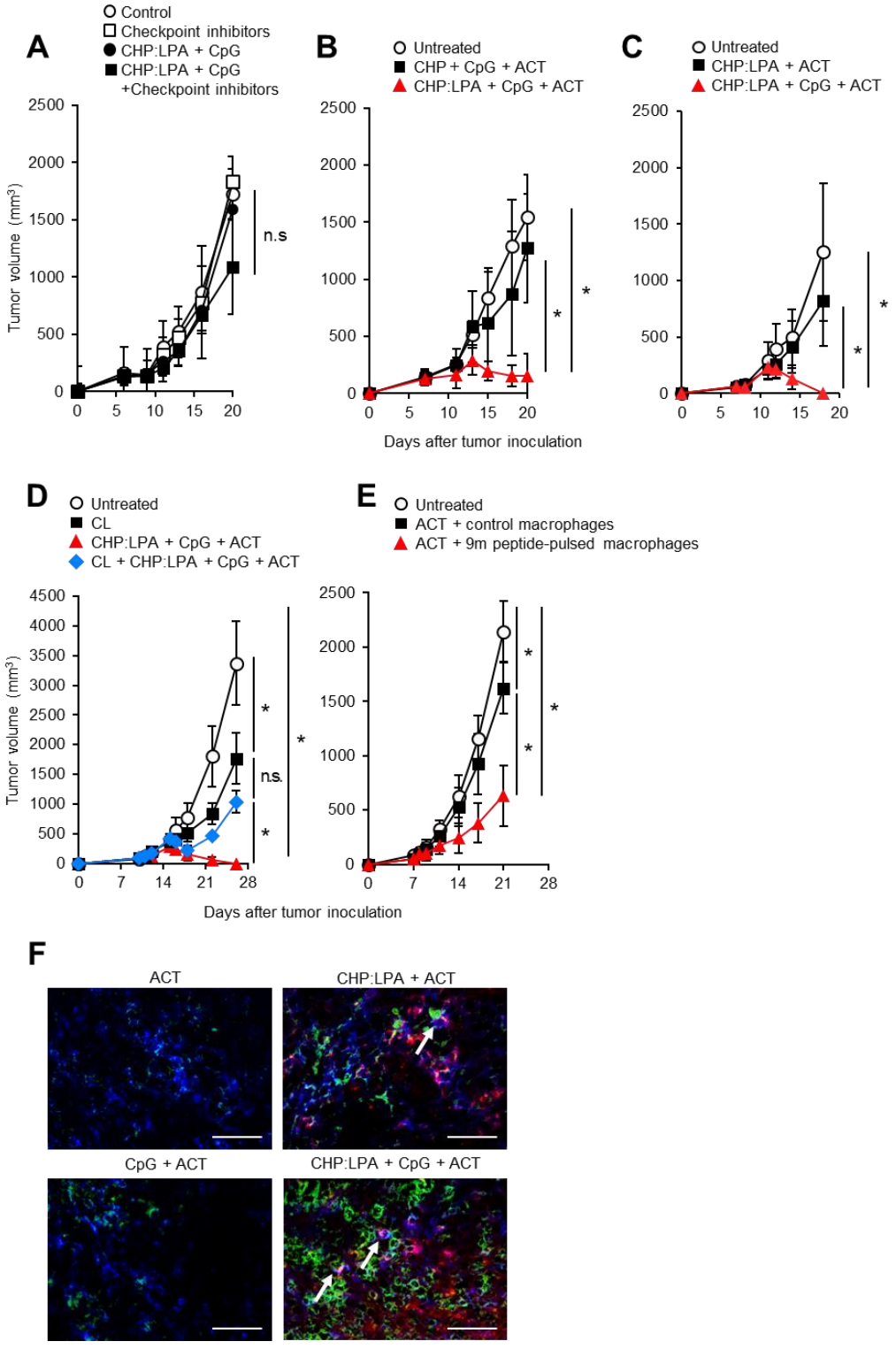
A
Control
Checkpoint inhibitors
CHP:LPA + CpG
CHP:LPA + CpG
+Checkpoint inhibitors
Tumor volume (mm3)
n.s
B
Untreated
CHP + CpG + ACT
CHP:LPA + CpG + ACT
Days after tumor inoculation
C
Untreated
CHP:LPA + ACT
CHP:LPA + CpG + ACT
D
Untreated
CL
CHP:LPA + CpG + ACT
CL + CHP:LPA + CpG + ACT
n.s.
E
Untreated
ACT + control macrophages
ACT + 9m peptide-pulsed macrophages
F
ACT
CHP:LPA + ACT
CpG + ACT
CHP:LPA + CpG + ACT

Figure 6. Induction of antigen presentation by TAMs improves tumor immune sensitivity. CMS5a cells were subcutaneously inoculated into BALB/c mice. The complex of CHP with 9m epitope-containing LPA (50 μg) was intravenously injected with CpG ODN (50 μg) into CMS5a tumor-bearing BALB/c mice on days 7 and 11. (**A**) Checkpoint inhibitors including anti-PD-1 (200 μg/mouse), anti-CTLA-4 (100 μg/mouse), and anti-GITR (200 μg/mouse) antibodies or isotype antibodies were intraperitoneally injected on days 7, 9, and 11 or (**B** to **F**) naïve $CD8^+$ cells isolated from DUC18 mice were infused on days 8 and 12 into the same mice. Tumor size was then monitored. (**D**) Clodronate liposomes (CL, 200 μl) were intravenously injected into CMS5a tumor-bearing mice on days 4 and 8, and other reagents were administered as in **B**. (**E**) CMS5a tumors were inoculated into BALB/c mice on day 0. Control or 9m peptide-pulsed bone marrow-derived macrophages were directly injected into the CMS5a tumor on days 6 and 10. DUC18 $CD8^+$ cells were infused on days 7 and 11. n = 8 to 10 per group. p-values were determined by Steel-Dwass test. *, $p < 0.05$. Experiments in A–E were performed at least two to three times with similar results. (**F**) Rhodamine-labeled CHP:LPA complex and CpG ODN were intravenously injected into CMS5a tumor-bearing BALB/c mice on day 7, followed by the infusion of DUC18/CD90.1 mouse-derived $CD8^+$ cells on day 8. Cryosections of the treated tumor were prepared and stained with anti-CD90.1 mAb (green). TAMs engulfing the labeled CHP:LPA complex are shown in red. Blue indicates $F4/80^+$ TAMs. The co-localization of CHP:LPA-ingested TAMs and specific $CD8^+$ T cells was indicated by arrows. The scale bar is 50 μm. These experiments were repeated twice with similar results.

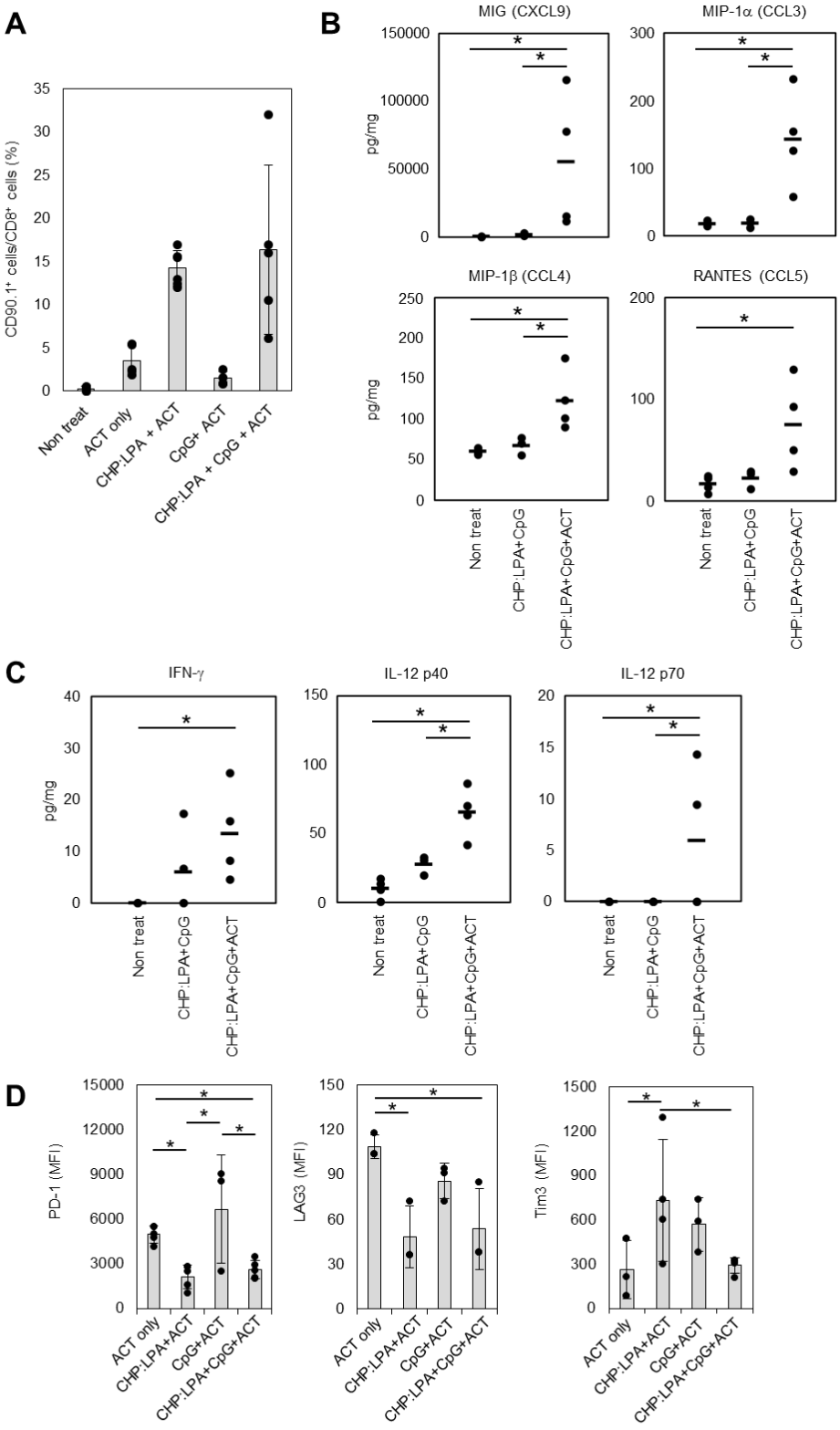
A
CD90.1+ cells/CD8+ cells (%)
Non treat
ACT only
CHP:LPA + ACT
CpG+ ACT
CHP:LPA + CpG + ACT
B
MIG (CXCL9)
MIP-1α (CCL3)
MIP-1β (CCL4)
RANTES (CCL5)
pg/mg
Non treat
CHP:LPA+CpG
CHP:LPA+CpG+ACT
C
IFN-γ
IL-12 p40
IL-12 p70
pg/mg
Non treat
CHP:LPA+CpG
CHP:LPA+CpG+ACT
D
PD-1 (MFI)
LAG3 (MFI)
Tim3 (MFI)
ACT only
CHP:LPA+ACT
CpG+ACT
CHP:LPA+CpG+ACT

Figure 7. Induction of antigen presentation by TAMs enhances accumulation of specific CD8$^+$ T cells at the tumor local site. (**A**) The complex of CHP with 9m epitope-containing LPA (50 μg) was intravenously injected with CpG ODN (50 μg) into CMS5a tumor-bearing BALB/c mice (two mice per group) on day 7. Naïve CD8$^+$ cells isolated from DUC18/CD90.1 mice were infused into the same mice on day 8. The tumors were removed from the mice on day 11, and frequency of CD90.1$^+$CD8$^+$ T cells in the tumors was determined by flow cytometry. Three experiments were pooled. The data show mean ± SD of three experiments. (**B** and **C**) CMS5a tumor-bearing BALB/c mice (n = 3 or 4 per group) were treated as same in **A**, and the tumors were isolated on day 11. The concentration of chemokines and cytokines in the tumors was measured by Bio-Plex assay. Circles in the graph shows the values of individual tumors and bars show mean. (**D**) Expression of immune checkpoint molecules on CD90.1$^+$CD8$^+$ T cells infiltrating in the tumors isolated on day 11 was analyzed by flow cytometry (n = 3 or 4 per group). Data are the mean ± SD. p-values were determined by a two-factor factorial ANOVA followed by Tukey-Kramer post hoc analysis. *, $p < 0.05$. These experiments were repeated at least two to three times with similar results.

< End of the document >